

Path Planning for Aerial Relays via Probabilistic Roadmaps

Pham Q. Viet and Daniel Romero

Dept. of Information and Communication Technology, University of Agder, Grimstad, Norway.

Email: {viet.q.pham,daniel.romero}@uia.no.

Abstract—Autonomous uncrewed aerial vehicles (UAVs) can be utilized as aerial relays to serve users far from terrestrial infrastructure. Unfortunately, existing algorithms for aerial relay path planning cannot accommodate general flight constraints or channel models. This is required in practice due to connectivity constraints, the presence of obstacles (e.g. buildings), and regulations. This paper proposes a framework that overcomes these limitations by spatially discretizing the flight region. To cope with the resulting exponential growth in complexity, the framework adopts a probabilistic roadmap approach, where a shortest path is found through a graph of randomly generated states. To attain high optimality with affordable complexity, the probability distribution used to generate these states is designed based on heuristic path planners with theoretical guarantees. The algorithms derived in this framework not only overcome the main limitations of existing schemes but also entail smaller computational complexity. Extensive theoretical and numerical results corroborate the merits of the proposed approach.

Index Terms—Aerial relays, path planning, probabilistic roadmaps, aerial communications.

I. INTRODUCTION

Autonomous uncrewed aerial vehicles (UAVs) received great attention in wireless communications due to their ability to extend the coverage of cellular networks [21], [33]. This need arises e.g. when terrestrial infrastructure is absent (as in remote areas), damaged by a natural or man-made disaster (as in military attacks), or not operational (as in the recent Spanish blackout [7]). In these situations, UAVs can be used to serve cellular users.

Several research problems emerge to address this need. For example, in *aerial base station (ABS) placement*, the goal is to find positions where the UAVs should hover to serve the users [21]. In this problem, the UAVs remain therefore static. However, some applications involve time-sensitive requirements (e.g. an avalanche warning must be delivered to users in a mountain) or moving users (e.g. a police pursuit). For those scenarios, one needs to plan the path of the UAVs to fly to suitable positions where they can serve the users. This is known as *relay path planning*.

This problem has spurred extensive recent research interest; see e.g. [6], [8], [10], [13], [14], [20], [24], [26]–[32]. However, as detailed in Sec. II, all existing schemes suffer from two main limitations:

- (L1) None of them can accommodate arbitrary flight constraints. Although they can often deal with convex constraints, flight regions in practice are non-convex due to the presence of obstacles (e.g. buildings and mountains) or no-fly zones (e.g. airports and military bases). Height limits in the EU and US are also specified with respect to the ground level, which results in non-convex regions whenever the terrain is not flat.
- (L2) No scheme can accommodate arbitrary channel models. In fact, the vast majority of them assume free-space propagation, which does not generally hold.

Furthermore, all existing schemes suffer from at least two of the following limitations: (L3) the paths of the relays are 2D, i.e. confined to a horizontal plane, (L4) they require that the users remain static, (L5) they can only handle one relay, (L6) their optimality cannot be guaranteed, and (L7) they cannot accommodate a general family of objective functions. See Table I and Sec. II for details.

The main contribution¹ of this paper is a *general framework for relay path planning* that addresses all the above

¹ Parts of this work have been presented at the IEEE Global Communications Conference 2023 [22]. Relative to that conference version, the present paper includes a generalization of the considered channel model to accommodate an arbitrary path loss exponent, an algorithm for serving moving users, additional objective functions, Theorem 2, an extension for more than 2 relays, an extension for more than 1 user, a complexity analysis, a large number of numerical experiments with additional benchmarks, and the analysis of the influence of the objective function on the UAV trajectory.

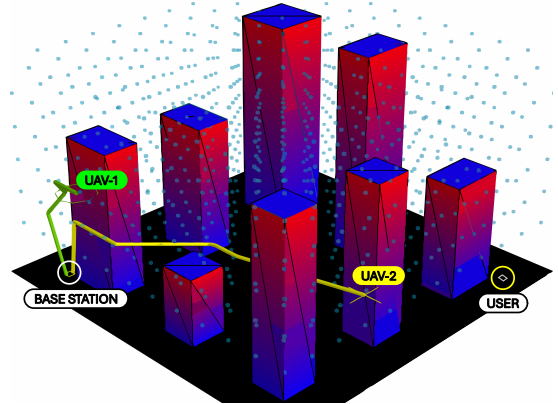


Fig. 1: Trajectories of two relay UAVs obtained with the proposed algorithm. Red/blue boxes represent buildings. The flight grid points are represented as blue dots. The green and yellow lines denote the trajectories of the UAVs.

TABLE I: Comparison of the proposed approach with existing works. * means that the sequence of iterates converges to a non-necessarily optimal solution.

	Objective	Arbitrary Flight Constraints	3D	Arbitrary Channel Model	Moving User	Multiple Relays	Theoretical Guarantees
[6], [24]	Maximize the minimum (across users) average (over time slots) rate.						*
[29]	Maximize the summation of the user's throughput in all time steps.				✓		*
[10]	Maximize the minimum (across terminal pairs) average (over time slots) rate.						*
[20]	Minimize the energy to relay given amounts of data in all pairs of users.						*
[32]	Minimize the sum (over all time slots) of the probability of outage.						*
[30]	Maximize the average (over all time slots) rate.					✓	*
[31]	Maximize the total amount of data received by the user.					✓	*
[14]	Maximize the minimum (across terminal pairs) average (over time slots) rate.		✓			✓	*
[8]	Minimize the (weighted) cumulative time needed to relay data of all terminal pairs.					✓	*
[13]	Minimize the flight time to relay data to all clusters of users.					✓	*
[26], [27]	Minimize the number of relay UAVs.				✓	✓	
[28]	Minimize the summation of flight distances.				✓	✓	
Proposed	Arbitrary additive objective.	✓	✓	✓	✓	✓	Optimality guarantees.

limitations. To understand the main idea, note that the reason why the aerial relay schemes in the *communications literature* cannot accommodate arbitrary flight constraints and channel models is that they do not discretize space. Treating the spatial coordinates as continuous variables facilitates planning the paths of multiple relays, but is only applicable in free space. On the other hand, the paths of UAVs in the *robotics literature* are typically planned in a discretized space; see e.g. [9]. This enables obstacle avoidance but hinders the usage of more than one relay due to the exponential growth of the number of possible states with respect to the number of UAVs and waypoints. Besides, these schemes cannot be applied to the relay path planning problem, which involves communication metrics and constraints, such as the need to maintain connectivity among the relays and with a terrestrial base station (BS) throughout the trajectories.

To combine the merits of both bodies of literature, this paper proposes *the first framework for relay path planning that is based on spatial discretization*. To cope with the exponential growth of the state space while accommodating communication constraints, the idea here is to adapt the *probabilistic roadmap* (PR) algorithm [11], which finds shortest-paths on graphs of randomly generated states. The adaptation is based on a custom probability distribution for generating these states, which in turn relies on a heuristic that produces feasible waypoint sequences. While the complexity of plain PR would grow exponentially with the number of UAVs, the complexity of the proposed algorithm grows just linearly.

The resulting framework, referred to as *PR with feasible initialization* (PRFI), features several strengths. First, (S1) PRFI can optimize arbitrary objectives so long as they are additive over time. (S2) These objectives, which will typically capture communication performance metrics, can involve arbitrary channel models, not necessarily the free-space model. The adopted objective is optimized subject to (S3) arbitrary constraints on the flight region and (S4) the constraint that the relays remain connected throughout their trajectories. In

addition, (S5) multiple relays and (S6) moving users can be accommodated. Finally, (S7) the optimality of PRFI can be established theoretically in certain cases.

The proposed PRFI framework is applied to three specific objectives: (i) the time it takes to establish connectivity with a user, (ii) the outage time, and (iii) the amount of transferred data. The case of a static user is treated separately since it allows greater optimality by avoiding uniform time discretization. An example in this scenario is shown in Fig. 1. The heuristic waypoint sequences used by PRFI are shown to be optimal in certain scenarios. Videos of trajectories can be found along with the developed simulator and simulation code at https://github.com/uiano/pr_for_relay_path_planning.

Sec. II summarizes the related work. Afterwards, Sec. III introduces the model and formulates the problem. The PR approach is then reviewed in Sec. IV. Specific PRFI algorithms are derived in Secs. V and VI and extensions are presented in Sec. VII. Finally, numerical experiments and conclusions are respectively presented in Secs. VIII and IX. Complete proofs of the theorems and further details can be found in [23].

Notation: Sets are notated by uppercase calligraphic letters. $|\mathcal{S}|$ is the cardinality of set \mathcal{S} . $\mathcal{A} \times \mathcal{B} \triangleq \{(a, b) : a \in \mathcal{A}, b \in \mathcal{B}\}$ is the Cartesian product of sets \mathcal{A} and \mathcal{B} , where (a, b) denotes a tuple. \mathbb{R}_+ is the set of non-negative real numbers. Boldface uppercase (lowercase) letters denote matrices (column vectors). $\|\mathbf{q}\|$ stands for the ℓ_2 -norm of vector \mathbf{q} . $\mathcal{I}[\cdot]$ is a function that returns 1 if the condition inside is true and 0 otherwise. $\min(a, b)$ and $\max(a, b)$ respectively denote the minimum and maximum between a and b . $\dot{\mathbf{q}}(t)$ stands for the entrywise first derivative of $\mathbf{q}(t)$ with respect to t . $\lfloor a \rfloor$ is the largest integer that is less than or equal to a .

II. RELATED WORK

The usage of UAVs in communications has attracted extensive research efforts. The problems considered in the literature can be classified into three main categories: ABS placement, path planning for data dissemination, and relay path planning.

In *ABS placement* [21], UAVs with onboard base stations hover at static locations to serve a typically large number of users; see [5], [19] and the references therein. The problem here is to determine the 3D locations of the ABSs.

In *path planning for data dissemination*, the UAVs receive data at a certain location, fly to another location, and then transmit the data; see e.g. [3] and the references therein.

In *relay path planning*, the UAVs establish links between terminals, possibly in multiple hops. The problem is to plan their paths. Many works focus on using a single UAV [6], [10], [20], [24], [29], [32] whereas others can accommodate multiple UAVs [8], [13], [14], [26]–[28], [30], [31]. Among these works, most consider free-space propagation [6], [10], [14], [20], [24], [26]–[31], but fading with arbitrary path loss exponents [32] and empirical air-to-ground channel models [8], [13] have also been considered. Existing schemes adopt one of the following three approaches: (i) non-linear optimization over continuous variables that represent the spatial coordinates of all UAVs [6], [10], [14], [20], [24], [29]–[32]; (ii) mixed integer linear programming (MILP) to determine the order in which a set of locations are visited following straight lines [8], [13]; and (iii) Steiner tree problem heuristics, which approximately minimize the number of required relays per time slot [26]–[28]. Table I summarizes the limitations of these schemes.

It is worth noting that there have been works where PR has been applied to UAV path planning (see e.g. [2] and references therein) but, to the best of our knowledge, never for communications. Furthermore, algorithms with spatial discretization have been considered for UAV communications (e.g. to plan a path through coverage areas [25]) but never for relay path planning.

III. THE PATH PLANNING PROBLEM

Consider a spatial region $\mathcal{S} \subset \mathbb{R}^3$ and let $\mathcal{F} \subset \mathcal{S}$ denote the set of points of \mathcal{S} above the ground and outside any building or obstacle. For simplicity, it is assumed that $[x, y, z]^\top \in \mathcal{F}$ whenever $[x, y, z']^\top \in \mathcal{F}$ for some $z' < z$, which essentially means that the buildings or obstacles contain no holes or parts that stand out.

A total of K aerial relays are deployed to establish a link between a base station (BS) at location $\mathbf{q}_{\text{BS}} \triangleq [x_{\text{BS}}, y_{\text{BS}}, z_{\text{BS}}]^\top \in \mathcal{S}$ and a collection of M users (UEs). To simplify the exposition, it will be initially assumed that $M = 1$; the case $M > 1$ is addressed in Sec. VII-B. The UE trajectory is denoted by the function $\mathbf{q}_{\text{UE}}(\cdot)$, defined by $t \mapsto \mathbf{q}_{\text{UE}}(t) \triangleq [x_{\text{UE}}(t), y_{\text{UE}}(t), z_{\text{UE}}(t)]^\top \in \mathcal{S}$, $t \geq 0$. Note that $\mathbf{q}_{\text{UE}}(\cdot)$ refers to a function whereas $\mathbf{q}_{\text{UE}}(t)$ is the vector that results from evaluating function $\mathbf{q}_{\text{UE}}(\cdot)$ at t .

Let $\bar{\mathcal{F}} \subset \mathcal{F}$ be the set of spatial locations where the UAVs can fly. This is typically determined by regulations (e.g. the minimum and maximum allowed altitudes, no-fly zones, and so on) and other operational constraints. The position of the k -th UAV at time t is represented as $\mathbf{q}_k(t) \in \bar{\mathcal{F}}$ and the positions of all UAVs at time t are collected into the $3 \times K$ matrix $\mathbf{Q}(t) \triangleq [\mathbf{q}_1(t), \dots, \mathbf{q}_K(t)]$, referred to as the *configuration point* (CP) at time t [11]. The set of all matrices whose

columns are in $\bar{\mathcal{F}}$ is the so-called *configuration space* (\mathcal{Q} -space) and will be denoted as \mathcal{Q} . The UAVs collectively follow a trajectory $\mathbf{Q}(\cdot)$, which is a function of the form $t \mapsto \mathbf{Q}(t) \in \mathcal{Q}$, $t \geq 0$. The take-off locations of the UAVs are collected in matrix $\mathbf{Q}_0 \triangleq \mathbf{Q}(0)$ and the maximum speed is v_{max} .

A. Communication Model

The targeted link must convey information in both ways but, to simplify the exposition, the focus here will be on the downlink. There, the signal transmitted by the BS is first decoded and retransmitted by UAV-1. The signal transmitted by UAV-1 is decoded and retransmitted by UAV-2 and so on, until the UE receives the signal retransmitted by UAV- K .

For the considered schemes, this communication can be implemented in many ways. However, the following assumption must be (at least approximately) satisfied:

(as) *the capacity of the channel between two terminals does not depend on the locations of the other terminals.*

Formally, if \mathbf{q}_k denotes the location of UAV- k at the time of transmission, (as) requires that the capacity $c(\mathbf{q}_{k-1}, \mathbf{q}_k)$ between UAV- $(k-1)$ and UAV- k does not depend on $\mathbf{q}_{k'}$ for $k' \neq k, k-1$. Equivalently, the interference that UAV- k receives from UAV- k' should be much smaller than the signal it receives from UAV- $(k-1)$. Note, nonetheless, that interference from any other transmitter in the environment can be readily included in $c(\mathbf{q}_{k-1}, \mathbf{q}_k)$ without violating (as).

The degree to which (as) holds depends on the allocation of communication resources (e.g. space, time, frequency, or code) to the UAVs². If, for example, $N_{\text{R}} = K + 1$ orthogonal resources are available, each UAV and the BS can use a different one and, as a result, (as) holds exactly. This case is not unrealistic in post-disaster scenarios where the terrestrial infrastructure is not operational and, therefore, available bandwidth abounds. Even if $N_{\text{R}} < K + 1$, (as) can approximately hold if only nearby UAVs use orthogonal resources. More generally, when N_{R} orthogonal resources are available, then UAV- k uses the same resource as UAV- $(k + iN_{\text{R}})$, $i = \pm 1, \pm 2, \dots$. Thus, UAV- k receives interference from UAV- $(k + iN_{\text{R}} - 1)$, $i = \pm 1, \pm 2, \dots$. These UAVs will generally be far away from UAV- k for moderate values of N_{R} and, therefore, the assumption will approximately hold.

Besides the data to be relayed towards the UE, each UAV consumes a rate r_{CC} for command and control. This means that the useful rate between the BS and UAV- k for a generic CP $\mathbf{Q} \triangleq [\mathbf{q}_1, \dots, \mathbf{q}_K]$ can be recursively obtained as

$$r_k(\mathbf{Q}) = \max(0, \min(r_{k-1}(\mathbf{Q}) - r_{\text{CC}}, c(\mathbf{q}_{k-1}, \mathbf{q}_k))). \quad (1)$$

Similarly, the achievable rate of the UE when it is at \mathbf{q}_{UE} is

$$r_{\text{UE}}(\mathbf{Q}, \mathbf{q}_{\text{UE}}) = \max(0, \min(r_K(\mathbf{Q}) - r_{\text{CC}}, c(\mathbf{q}_K, \mathbf{q}_{\text{UE}}))). \quad (2)$$

The second argument in r_{UE} will be omitted when it is clear from the context. Throughout the trajectory, the UAVs must have connectivity with the BS, meaning that $r_k(\mathbf{Q}(t)) \geq r_{\text{CC}} \forall k, t$.

²Inter-hop interference can also be mitigated via directional antennas or beamforming, power control, and interference cancellation at the receivers.

B. Capacity Maps

A *capacity map* is a function c that maps a pair of locations \mathbf{q} and \mathbf{q}' to the capacity $c(\mathbf{q}, \mathbf{q}')$ of the channel between them. This capacity can be expressed in terms of the channel gain $\gamma(\mathbf{q}, \mathbf{q}')$ between \mathbf{q} and \mathbf{q}' as

$$c(\mathbf{q}, \mathbf{q}') = c_{\text{SNR}}(\gamma(\mathbf{q}, \mathbf{q}')) \triangleq B \log_2(1 + \gamma(\mathbf{q}, \mathbf{q}')/\sigma^2), \quad (3)$$

where B is the bandwidth and σ^2 captures both interference and noise power.

There are many approaches to obtain function γ . One can, for example, rely on 3D terrain/city models together with ray-tracing algorithms or other simulation software. If such models are not available, one may construct a channel-gain radio map using measurements [17]. To this end, the most common approach builds upon the so-called *tomographic model* [16], [18], which prescribes that

$$\gamma(\mathbf{q}, \mathbf{q}') = \gamma_{\text{PL}}(d(\mathbf{q}, \mathbf{q}')) \cdot 10^{\gamma_{\text{abs}}^{\text{dB}}(\mathbf{q}, \mathbf{q}')/10}, \quad (4)$$

where $d(\mathbf{q}, \mathbf{q}') \triangleq \|\mathbf{q} - \mathbf{q}'\|$, $\gamma_{\text{PL}}(d)$ is the *path loss* of a link with distance d , and $\gamma_{\text{abs}}^{\text{dB}}(\mathbf{q}, \mathbf{q}')$ is the gain due to absorption. Specifically,

$$\gamma_{\text{PL}}(d) \triangleq P_t G_t G_r \left(\frac{\lambda}{4\pi d} \right)^\beta, \quad (5)$$

where P_t , G_t , G_r , λ , and β are respectively the transmit power, transmit gain, receive gain, wavelength, and pathloss exponent. On the other hand, $\gamma_{\text{abs}}^{\text{dB}}(\mathbf{q}, \mathbf{q}')$ is given by the line integral [16]

$$\gamma_{\text{abs}}^{\text{dB}}(\mathbf{q}, \mathbf{q}') \triangleq - \frac{1}{\sqrt{d(\mathbf{q}, \mathbf{q}')}} \int_{\mathbf{q}}^{\mathbf{q}'} s(\zeta) d\zeta, \quad (6)$$

where s is the so-called *spatial loss field* (SLF), which quantifies absorption at each spatial location. Clearly, $s(\zeta)$ is 0 if there is no obstacle at ζ .

The proposed algorithm can accommodate *arbitrary capacity maps*, not necessarily based on ray-tracing or the tomographic model. However, some theoretical results will rely on a limit case of tomographic maps referred to as the *tomographic map with infinite absorption* (TMIA), where $s(\zeta) \in \{0, \infty\} \forall \zeta$. Clearly, in this case,

$$c(\mathbf{q}, \mathbf{q}') = \begin{cases} \bar{c}(d(\mathbf{q}, \mathbf{q}')), & \text{if there is LOS between } \mathbf{q} \text{ and } \mathbf{q}' \\ 0 & \text{otherwise,} \end{cases} \quad (7)$$

where $\bar{c}(\cdot) \triangleq c_{\text{SNR}}(\gamma_{\text{PL}}(\cdot))$. This corresponds to an environment where the obstacles (e.g. buildings) are opaque to radio waves, an accurate assumption in high frequencies; e.g. in mmWave bands [19]. A map of this kind has been used in the related literature; see e.g. [4]. It is convenient for theoretical derivations since it essentially constitutes a worst-case map.

Remark 1: The actual channel between two spatial locations can be worse than that predicted by the adopted capacity map. It may be thus convenient to include a safety margin in the computations to ensure connectivity.

C. Problem Formulation

This paper addresses the problem of designing the trajectory of the UAVs so that they can serve the UE(s). Given \mathbf{q}_{BS} , $\mathbf{Q}_0 \in \mathcal{Q}$, $\mathbf{q}_{\text{UE}}(\cdot)$, K , c , r_{CC} , and v_{max} , the problem is to solve

$$\underset{\mathbf{Q}(\cdot)}{\text{minimize}} \quad J(\mathbf{Q}(\cdot)) \quad (8a)$$

$$\text{s.t.} \quad \mathbf{Q}(t) \in \mathcal{Q} \quad \forall t, \quad \mathbf{Q}(0) = \mathbf{Q}_0 \quad (8b)$$

$$r_k(\mathbf{Q}(t)) \geq r_{\text{CC}} \quad \forall k, t \quad (8c)$$

$$\|\dot{\mathbf{q}}_k(t)\| \leq v_{\text{max}} \quad \forall k, t, \quad (8d)$$

where the objective function J is discussed next. Observe that the optimization variable $\mathbf{Q}(\cdot)$ is a function of the continuous-time variable t . Note also that (8) does not enforce a minimum distance between UAVs. Such a constraint is omitted for simplicity but can be accommodated in the proposed scheme.

The following objective functions will be considered:

- **Connection time.** In many situations, it is desirable to establish connectivity between the UE and the BS as soon as possible. This is the case when time-sensitive information must be delivered in a short time, e.g. to notify a user of a tsunami, earthquake, or military attack. The goal is, therefore, to minimize the *connection time*

$$J(\mathbf{Q}(\cdot)) = T_c(\mathbf{Q}(\cdot)) \triangleq \inf\{t : r_{\text{UE}}(\mathbf{Q}(t), \mathbf{q}_{\text{UE}}(t)) \geq r_{\text{UE}}^{\text{min}}\}, \quad (9)$$

where $r_{\text{UE}}^{\text{min}}$ is the target rate. Note that, consistent with the standard convention for the infimum, $T_c(\mathbf{Q}(\cdot)) = \infty$ if $r_{\text{UE}}(\mathbf{Q}(t), \mathbf{q}_{\text{UE}}(t)) < r_{\text{UE}}^{\text{min}}$ for all t . Note also that $J(\mathbf{Q}(\cdot))$ is not meaningful if the UE loses connectivity after the connection is established, which can happen if the UE moves. This renders this objective immaterial unless the UE is static.

- **Outage time.** A natural objective when the UE is not static is the time during which it has no connectivity [12]. This motivates minimizing the *outage time*

$$J(\mathbf{Q}(\cdot)) = \int_0^T \mathcal{I}[r_{\text{UE}}(\mathbf{Q}(t), \mathbf{q}_{\text{UE}}(t)) < r_{\text{UE}}^{\text{min}}] dt, \quad (10)$$

where T is the time horizon and $\mathcal{I}[\cdot]$ was defined in Sec. I.

- **Transferred data.** In some applications, data may be relatively delay tolerant. Thus, instead of minimizing outage time, one may be interested in maximizing the total amount of data received by the UE within a given time horizon T . This gives rise to the objective function

$$J(\mathbf{Q}(\cdot)) = - \int_0^T r_{\text{UE}}(\mathbf{Q}(t), \mathbf{q}_{\text{UE}}(t)) dt, \quad (11)$$

where the minus sign is due to the fact that (8) is a minimization problem.

Clearly, the choice of objective determines the optimal trajectory. An analysis of this influence is presented in Appendix A.

IV. PATH PLANNING VIA PROBABILISTIC ROADMAPS

Since Problem (8) involves optimization with respect to a trajectory, which comprises infinitely many CPs, the exact

solution cannot generally be found by numerical means. For this reason, both space and time will be discretized.

Specifically, the flight region $\bar{\mathcal{F}}$ is discretized into a regular 3D *flight grid* $\bar{\mathcal{F}}_G \subset \bar{\mathcal{F}} \subset \mathbb{R}^3$, whose points are separated along the x, y, and z axes respectively by δ_x , δ_y , and δ_z ; see Fig. 1. To simplify some expressions, it will be assumed that the take-off locations of the UAVs are in $\bar{\mathcal{F}}_G$. This spatial discretization also induces a grid \mathcal{Q}_G in the Q-space, which e.g. for $K = 2$ is given by $\mathcal{Q}_G \triangleq \bar{\mathcal{F}}_G \times \bar{\mathcal{F}}_G$.

Regarding the time-domain discretization, the trajectory $\mathbf{Q}(\cdot)$ will be designed by first finding a CP sequence $P \triangleq \{\mathbf{Q}[0], \dots, \mathbf{Q}[N-1]\}$ through the grid \mathcal{Q}_G . This sequence will be referred to as *combined path*, whereas the waypoint sequence $\mathbf{q}_k[n]$ that each individual UAV must follow will be referred to as a *path*. Given P , the trajectory $\mathbf{Q}(\cdot)$ is recovered by interpolating the waypoints in P . A path P will be said to be *feasible* iff the associated trajectory $\mathbf{Q}(\cdot)$ is feasible.

Having introduced the discretization, the next step is to discuss how to obtain a feasible waypoint sequence that attains a satisfactory objective value. Conventional algorithms for planning the path of a single (non-relay) UAV create a graph whose nodes are the points of $\bar{\mathcal{F}}_G$ and where an edge exists between two nodes if the associated points are adjacent on the grid. In a 3D regular grid like $\bar{\mathcal{F}}_G$, each point has typically 26 adjacent points, which renders the application of shortest-path algorithms on such a graph viable. However, the grid \mathcal{Q}_G has exponentially many more points than $\bar{\mathcal{F}}_G$. For example, if $\bar{\mathcal{F}}_G$ is a (small) $10 \times 10 \times 10$ grid, then \mathcal{Q}_G has 10^{3K} points. Besides, since each of them has generally $27^K - 1$ adjacent points, solving (8) via shortest-path algorithms is prohibitive.

To bypass this kind of difficulties in other contexts, the seminal paper [11] proposed the PR algorithm, which consists of 3 steps: Step 1: a node set $\mathcal{N} \subset \mathcal{Q}$ with a much smaller number of nodes than \mathcal{Q}_G is randomly generated. Step 2: the edge set $\mathcal{E} \subset \mathcal{N} \times \mathcal{N}$ is constructed by connecting the nodes corresponding to CPs \mathbf{Q} and \mathbf{Q}' if (i) they are nearest neighbors and (ii) it is possible to transition directly from \mathbf{Q} to \mathbf{Q}' . Step 3: a shortest path is found on the graph with node set \mathcal{N} and edge set \mathcal{E} .

Unfortunately, even though the number of CPs in \mathcal{N} is significantly smaller than in \mathcal{Q}_G , it will still be prohibitive for the application at hand. This is because plain vanilla PR generates the CPs uniformly at random over the configuration space and, thus, the the number of CPs necessary to find a feasible (let alone satisfactory) path grows exponentially with the dimensionality of the configuration space.

The main idea of this paper is to modify PR to counteract this limitation: instead of generating the CPs according to a uniform distribution in Step 1, a special probability distribution is developed to ensure that a feasible waypoint sequence can be found by drawing a nearly minimal number of CPs.

V. PATH PLANNING FOR A STATIC UE

This section addresses the path planning problem for a single static UE. The case of a single moving UE is addressed in Sec. VI. Multiple UEs will be considered in Sec. VII-B.

Although a static UE is a special case of a moving UE where $\mathbf{q}_{\text{UE}}(t) = \mathbf{q}_{\text{UE}} \forall t$, it is useful to first address the static

scenario because it simplifies the presentation and yields an algorithm that attains greater optimality. It is also convenient to focus on the connection time objective (9). Minimizing the outage time (10) is equivalent since the UE is static. In turn, maximizing the transferred data is deferred to Sec. VI because the approach there is more suitable to enforce the time horizon in (11) as it involves uniform time discretization.

A. Planning the Tentative Path

As indicated in Sec. IV, the proposed framework adapts PR by mainly modifying the probability distribution for CP generation. As detailed next, this distribution relies on a heuristic that produces a feasible path.

A trajectory $\mathbf{Q}(\cdot)$ is said to be *valid* if it is feasible and attains a finite connection time $T_c(\mathbf{Q}(\cdot))$. Equivalently, a combined path $P \triangleq \{\mathbf{Q}[0], \dots, \mathbf{Q}[N-1]\}$ is valid if it is feasible and $\exists n : r_{\text{UE}}(\mathbf{Q}[n]) \geq r_{\text{UE}}^{\min}$. A feasible path P on a grid \mathcal{Q}_G is said to be *optimal* if it attains the lowest connection time among all feasible paths on \mathcal{Q}_G . The heuristic proposed in this section will be seen to produce a *valid* (and sometimes even *optimal*) path under general conditions.

Interestingly, $K = 2$ UAVs often suffice to guarantee the existence of a valid path. This is the case e.g. if h and d are not too large relative to r_{UE}^{\min} and r_{CC} , where h is the height of the highest obstacle and $d \triangleq \sqrt{(x_{\text{UE}} - x_{\text{BS}})^2 + (y_{\text{UE}} - y_{\text{BS}})^2}$ is the horizontal distance between the BS and the UE:

Proposition 1: Let c be a TMA map. Suppose that $\mathbf{q}_k(0) = \mathbf{q}_{\text{BS}} \forall k$ and that the UAVs can fly above h . If $h < \min(z_{\text{UE}} + \bar{c}^{-1}(r_{\text{UE}}^{\min}), z_{\text{BS}} + \bar{c}^{-1}(r_{\text{UE}}^{\min} + 2r_{\text{CC}}))$ and $d \leq \bar{c}^{-1}(r_{\text{UE}}^{\min} + r_{\text{CC}})$, then there exists a valid path with $K = 2$.

Proof: Let $z \triangleq \min(z_{\text{UE}} + \bar{c}^{-1}(r_{\text{UE}}^{\min}), z_{\text{BS}} + \bar{c}^{-1}(r_{\text{UE}}^{\min} + 2r_{\text{CC}}))$ and suppose that $K = 2$. It is easy to show that if UAV-1 flies to $\mathbf{q}_1 \triangleq [x_{\text{BS}}, y_{\text{BS}}, z]^T$ and UAV-2 flies first to \mathbf{q}_1 and later to $\mathbf{q}_2 \triangleq [x_{\text{UE}}, y_{\text{UE}}, z]^T$, the resulting trajectory $\mathbf{Q}(\cdot)$ is feasible and $T_c(\mathbf{Q}(\cdot)) < (z - z_{\text{BS}} + d)/v_{\text{max}} < +\infty$. ■

Note that this sufficient condition enjoys great generality because it relies on a worst-case map. Therefore, the case $K = 2$ is of special relevance. Since it is also easier to understand, the rest of this section assumes $K = 2$; the extension to $K > 2$ is addressed in Sec. VII-A.

The proof of Proposition 1 is constructive and, therefore, provides a valid path. However, to apply PR it is preferable to adopt the approach described next since it yields a valid path that attains a significantly smaller objective; cf. Sec. VIII. This approach first generates the path for UAV-2. Then, a path is found for UAV-1 to serve UAV-2 all the way. If this is not possible, the path of UAV-2 is *lifted* until UAV-2 can be served.

Before delving into the details of the procedure, some notation and terminology needs to be introduced. Let $\mathcal{R}(\mathbf{q}, r) \triangleq \{\mathbf{q}' \in \bar{\mathcal{F}}_G : c(\mathbf{q}, \mathbf{q}') \geq r\}$ and note that, for a path to be valid, it is necessary (but not sufficient) that UAV-1 is in $\mathcal{R}(\mathbf{q}_{\text{BS}}, 2r_{\text{CC}})$ throughout the path and in $\mathcal{R}(\mathbf{q}_{\text{BS}}, 2r_{\text{CC}} + r_{\text{UE}}^{\min})$ at the moment of establishing connectivity with the UE. Similarly, let $\mathcal{R}(\mathbf{q}, r, r') \triangleq \{\mathbf{q}'' \in \bar{\mathcal{F}}_G \mid \exists \mathbf{q}' \in \mathcal{R}(\mathbf{q}, r) : c(\mathbf{q}', \mathbf{q}'') \geq r'\}$, and note that, for a path to be valid, it is necessary (not sufficient) that UAV-2 is in $\mathcal{N}_2 \triangleq \mathcal{R}(\mathbf{q}_{\text{BS}}, 2r_{\text{CC}}, r_{\text{CC}})$ throughout the path and in $\mathcal{D}_2 \triangleq \mathcal{R}(\mathbf{q}_{\text{BS}}, 2r_{\text{CC}} + r_{\text{UE}}^{\min}, r_{\text{CC}} + r_{\text{UE}}^{\min}) \cap \mathcal{R}(\mathbf{q}_{\text{UE}}, r_{\text{UE}}^{\min})$ at the moment of establishing connectivity with the UE.

Theorem 1: Let $\bar{\mathcal{F}}_G$ be a sufficiently dense regular grid and let $\mathbf{Q}[0] = [\mathbf{q}_{BS}, \mathbf{q}_{BS}]$. Suppose that c is a TMIA map and

$$h_{max} \leq \sqrt{[\bar{c}^{-1}(2r_{CC})]^2 - [\bar{c}^{-1}(2r_{CC} + r_{UE}^{min})]^2} \quad (13)$$

$$r_{UE}^{min} \geq B \log_2 \left(\frac{1 + 2^\beta SNR_{cc}^{min}}{1 + SNR_{cc}^{min}} \right), \quad (14)$$

where $SNR_{cc}^{min} \triangleq 2^{r_{cc}/B} - 1$. If a valid path for (8) exists through waypoints in \mathcal{Q}_G , then the tentative path $P^V \triangleq \{\mathbf{q}_1[i], \hat{\mathbf{q}}_2[n_i], i = 0, \dots, \tilde{N} - 1\}$ obtained from Algorithm 2 is valid.

Proof: See Appendix B. ■

Thus, if r_{UE}^{min} and r_{CC} are not too large relative to the size of the region, the approach in this section results in a valid combined path whenever such a path exists.

B. Probabilistic Roadmaps with Feasible Initialization

This section adapts PR to solve (8) by relying on the tentative path produced by Algorithm 2.

1) *Construction of the Node Set:* As described earlier, the first step in PR is to randomly generate a set \mathcal{N} of CPs. The sampled distribution drastically impacts the optimality of the resulting combined path and the computational burden of the algorithm. In the work at hand, \mathcal{N} will comprise all the CPs of the path $P^V = \{\mathbf{Q}[0], \dots, \mathbf{Q}[\tilde{N} - 1]\}$ from Sec. V-A together with C additional CPs drawn at random around the CPs in P^V .

Specifically, for each $\mathbf{Q} = [\mathbf{q}_1, \mathbf{q}_2] \in P^V$, the proposed sampling strategy generates $\lfloor C/\tilde{N} \rfloor$ configuration points $\tilde{\mathbf{Q}} = [\tilde{\mathbf{q}}_1, \tilde{\mathbf{q}}_2]$ as follows. First, generate $\tilde{\mathbf{q}}_1$ by drawing a point of $\mathcal{R}(\mathbf{q}_{BS}, 2r_{CC}) - \{\mathbf{q}_1\}$ with probability proportional to $1/\|\tilde{\mathbf{q}}_1 - \mathbf{q}_1\|$. Next, independently of $\tilde{\mathbf{q}}_1$, generate $\tilde{\mathbf{q}}_2$ by drawing a point of $\mathcal{R}(\mathbf{q}_{BS}, 2r_{CC}, r_{CC}) - \{\mathbf{q}_2\}$ with probability proportional to $1/\|\tilde{\mathbf{q}}_2 - \mathbf{q}_2\|$. If $\tilde{\mathbf{q}}_2 \notin \mathcal{R}(\tilde{\mathbf{q}}_1, r_{CC})$, another pair $(\tilde{\mathbf{q}}_1, \tilde{\mathbf{q}}_2)$ is generated until $\tilde{\mathbf{q}}_2 \in \mathcal{R}(\tilde{\mathbf{q}}_1, r_{CC})$, which will eventually happen since $\tilde{\mathbf{q}}_2 \in \mathcal{R}(\mathbf{q}_{BS}, 2r_{CC}, r_{CC})$.

This procedure, which is based on the distance to CPs in P^V , ensures that many of the sampled CPs lie close to the tentative path while others may be farther away, thereby increasing the chances for finding nearly optimal paths.

2) *Construction of the Edge Set:* The next step is to construct the edge set of a nearest neighbor graph whose node set was generated in Sec. V-B1. To obtain trajectories with a lower connection time, it is convenient not to require that each UAV moves through adjacent points in $\bar{\mathcal{F}}_G$: what matters is that the UAVs can move from one CP to another (i) without losing connectivity and (ii) without abandoning $\bar{\mathcal{F}}$. Thus, an edge $(\mathbf{Q}, \mathbf{Q}')$ is added to the edge set if \mathbf{Q} and \mathbf{Q}' are nearest neighbors and conditions (i) and (ii) are satisfied. To numerically check (i) and (ii), one can verify that they hold for a finite set of points in the line segment between \mathbf{Q} and \mathbf{Q}' .

Since the objective is the connection time, the weight of an edge between $\mathbf{Q} = [\mathbf{q}_1, \mathbf{q}_2]$ and $\mathbf{Q}' = [\mathbf{q}'_1, \mathbf{q}'_2]$ will be given by the time that the UAVs require to move from \mathbf{Q} to \mathbf{Q}' . Given the speed constraint (8d), this time is determined by the UAV that traverses the longest distance and, therefore, equals $\max_k \|\mathbf{q}_k - \mathbf{q}'_k\|/v_{max}$.

Algorithm 1: Tentative Path UAV-2, Static UE

input: $\bar{\mathcal{F}}_G, \mathbf{q}_{BS}, \mathbf{q}_{UE}, \mathbf{q}_2[0], r_{CC}, r_{UE}^{min}, c$

- 1: Find the candidate locations of UAV-2
→ $\mathcal{N}_2 = \mathcal{R}(\mathbf{q}_{BS}, 2r_{CC}, r_{CC})$
- 2: Find the destinations of UAV-2
→ $\mathcal{D}_2 = \mathcal{R}(\mathbf{q}_{BS}, 2r_{CC} + r_{UE}^{min}, r_{CC} + r_{UE}^{min}) \cap \mathcal{R}(\mathbf{q}_{UE}, r_{UE}^{min})$
- 3: Construct graph \mathcal{G}_1 with weights $w(\mathbf{q}, \mathbf{q}') = \|\mathbf{q} - \mathbf{q}'\|$
- 4: **return** $p_2 \triangleq \text{shortest_path}(\mathbf{q}_2[0], \mathcal{D}_2)$

3) *Path Planning in Q-Space:* After the nearest-neighbor graph is constructed, a shortest path is sought from \mathbf{Q}_0 to any of the CPs $[\mathbf{q}_1, \mathbf{q}_2]$ that satisfy $\mathbf{q}_1 \in \mathcal{R}(\mathbf{q}_{BS}, 2r_{CC} + r_{UE}^{min})$ and $\mathbf{q}_2 \in \mathcal{R}(\mathbf{q}_1, r_{CC} + r_{UE}^{min}) \cap \mathcal{R}(\mathbf{q}_{UE}, r_{UE}^{min})$. The resulting CP sequence P^{PR} will never have a greater objective than the tentative path P^V provided that all consecutive CPs in P^V are connected in the PR graph. This holds so long as the number of neighbors in Sec. V-B2 is not too low.

C. From the Waypoint Sequence to the Trajectory

Given the waypoint sequence $P^{PR} = \{\mathbf{Q}[0], \dots, \mathbf{Q}[N^{PR} - 1]\}$ obtained in the previous step, it remains only to obtain the trajectory $\mathbf{Q}(\cdot)$. To this end, it is necessary to determine the time at which the UAVs arrive at each of the waypoints $\mathbf{Q}[n]$. As indicated in Sec. V-B3, the time it takes to arrive at $\mathbf{Q}[n] = [\mathbf{q}_1[n], \mathbf{q}_2[n]]$ from $\mathbf{Q}[n-1] = [\mathbf{q}_1[n-1], \mathbf{q}_2[n-1]]$ is $\max_k \|\mathbf{q}_k[n] - \mathbf{q}_k[n-1]\|/v_{max}$. Let t_n represent the time at which all the UAVs arrive at $\mathbf{Q}[n]$ and let $t_0 = 0$. In this case, it clearly holds that

$$t_n = t_{n-1} + \frac{\max_k \|\mathbf{q}_k[n] - \mathbf{q}_k[n-1]\|}{v_{max}}. \quad (15)$$

This provides $\mathbf{Q}(t_n) = \mathbf{Q}[n]$ for $n = 0, \dots, N^{PR} - 1$. For $t \geq t_{N^{PR}-1}$, one can simply set $\mathbf{Q}(t) = \mathbf{Q}(t_{N^{PR}-1})$. The CPs $\mathbf{Q}(t)$ for other values of t will be determined by the flight controller, which may be provided just a sequence of waypoints along with their times. For simulation, one can use linear interpolation to resample $\mathbf{Q}(\cdot)$ at uniform intervals.

Note that, if no lifting steps are used and UAV-2 travels at full speed all the time, the trajectory obtained by applying (15) directly on the tentative path is optimal among all trajectories through adjacent gridpoints in $\bar{\mathcal{F}}_G$. This is because no other such a trajectory can attain UE connectivity in a shorter time. The trajectory returned by PRFI will thereby be optimal up to the suboptimality introduced by the spatial discretization.

The scheme is summarized as Algorithm 3 and will be referred to as *PR with feasible initialization* (PRFI) for static UE. Generalizations to $K > 2$ and more than one UE are respectively presented in Secs. VII-A and VII-B. The complexity analysis can be found in Sec. VII-C.

Remark 2: To ensure that the UAVs properly follow the planned trajectories, their on-board localization and synchronization systems should be sufficiently accurate. If, e.g. due to wind or unexpected obstacles, a UAV cannot reach a planned waypoint on time, it should inform the rest so they wait and connectivity is maintained. Replanning may be necessary.

Algorithm 2: Tentative Path UAV-1, Static UE

input: $\bar{\mathcal{F}}_G, \mathbf{q}_{BS}, \mathbf{q}_{UE}, \mathbf{q}_1[0], p_2, r_{CC}, r_{UE}^{\min}, c$

- 1: **for** $u = 0, 1, \dots, \tilde{N}$ **do**
- 2: $\{\hat{\mathbf{q}}_2[0], \hat{\mathbf{q}}_2[1], \dots, \hat{\mathbf{q}}_2[\tilde{N}_u - 1]\} \triangleq L^{(u)}(p_2)$
- 3: Find candidate locations of UAV-1
 $\rightarrow \mathcal{N}_1[n] = \mathcal{R}(\mathbf{q}_{BS}, 2r_{CC}) \cap \mathcal{R}(\hat{\mathbf{q}}_2[n], r_{CC})$
- 4: Find destinations of UAV-1 $\rightarrow \mathcal{D}_1 =$
 $\mathcal{R}(\mathbf{q}_{BS}, 2r_{CC} + r_{UE}^{\min}) \cap \mathcal{R}(\hat{\mathbf{q}}_2[\tilde{N}_u - 1], r_{CC} + r_{UE}^{\min})$
- 5: Construct extended graph \mathcal{G}_2 with weights as in Sec. V-A2.
- 6: **if** path_exists($(0, \mathbf{q}_1[0]), \mathbb{N} \times \mathcal{D}_1$) **then**
- 7: $\{(n_0, \mathbf{q}_1[0]), (n_1, \mathbf{q}_1[1]), \dots, (n_{\tilde{N}-1}, \mathbf{q}_1[\tilde{N} - 1])\}$
 \triangleq shortest_path($(0, \mathbf{q}_1[0]), \mathbb{N} \times \mathcal{D}_1$)
- 8: Obtain $\mathbf{Q}[\tilde{n}] = [\mathbf{q}_1[\tilde{n}], \hat{\mathbf{q}}_2[n_{\tilde{n}}]]$, $\tilde{n} = 0, 1, \dots, \tilde{N} - 1$
- 9: **return** $P^V = \{\mathbf{Q}[0], \mathbf{Q}[1], \dots, \mathbf{Q}[\tilde{N} - 1]\}$
- 10: **end if**
- 11: **end for**

Algorithm 3: PRFI for Static UE

input: $\bar{\mathcal{F}}_G, \mathbf{q}_{BS}, \mathbf{q}_{UE}, \mathbf{Q}_0, C, v_{\max}, r_{CC}, r_{UE}^{\min}, c$

- 1: $p_2 \triangleq$ tentative path for UAV-2 via Algorithm 1
- 2: $P^V \triangleq$ combined tentative path via Algorithm 2
- 3: For each $\mathbf{Q} \in P^V$, draw $\lfloor C/\tilde{N} \rfloor$ CPs $\rightarrow \mathcal{N}$
- 4: Construct a nearest-neighbor graph from \mathcal{N}
- 5: $P^{PR} \triangleq$ shortest_path($\mathbf{Q}_0, \{\mathbf{Q} \in \mathcal{N} : r_{UE}(\mathbf{Q}) \geq r_{UE}^{\min}\}$)
- 6: Compute waypoints $\{(t_n, \mathbf{Q}(t_n))\}_n$ as in Sec. V-C
- 7: **return** $\{(t_n, \mathbf{Q}(t_n))\}_n$

Remark 3: For deployments in dynamic environments, it is convenient to (i) estimate the capacity map frequently with measurements collected by the UAVs themselves and to (ii) replan the trajectories whenever the capacity map estimate is updated. This may be crucial to guarantee connectivity since obstacles may move or new obstacles appear.

VI. PATH PLANNING FOR MOVING UE

This section solves (8) when the UE moves. Since minimizing the connection time is not meaningful in this scenario (cf. Sec. III-C), the focus will be on optimizing the outage time (10) and the amount of transferred data (11).

Along the lines of Sec. V, the algorithm here is referred to as *PRFI for moving UE* and also adapts PR to find a path in Q-space given a tentative path. However, the algorithm developed in this section significantly differs from the one in Sec. V due to the different temporal dynamics of the problems they address: whereas in Sec. V the UAVs must move at maximum speed to reach the destination as fast as possible, in the case of a moving UE, the time at which the UAVs must arrive at each waypoint is dictated by the trajectory of the UE. For this reason, the paths of the UE and UAVs will be obtained by sampling their trajectories at a regular interval τ . Specifically, the path of the UE will be represented as $p_{UE} := \{\mathbf{q}_{UE}[0], \mathbf{q}_{UE}[1], \dots, \mathbf{q}_{UE}[N_{UE} - 1]\}$, where $\mathbf{q}_{UE}[n] = \mathbf{q}_{UE}(n\tau)$, $n = 0, \dots, N_{UE} - 1$. Similarly, the paths of the UAVs will be planned in such a way that each one

is at a point of $\bar{\mathcal{F}}_G$ at every sampling instant. This requires that τ is small enough so that the UAVs can move from one grid point to any adjacent one in this time.

A. Planning the Tentative Path

As in Sec. V, the explanation will assume $K = 2$ UAVs; the case $K > 2$ is addressed in Sec. VII-A.

Recall that the closer the tentative path to the optimal combined path, the greater the optimality of the combined path returned by PR. Therefore, it is desirable that the tentative path approximately minimizes the adopted metric. In the case of the outage time, this can be readily accomplished by planning the path of both UAVs separately along the lines of Sec. V. However, when the metric is the one in (11), such an approach is not viable because the UE rate is a function of the positions of both UAVs. As noted in Sec. IV, planning such a path jointly would be computationally prohibitive. Thus, with this metric, the tentative path will still be planned to minimize the outage time. PR will then optimize the path in Q-space to maximize the metric in (11).

1) *Path for UAV-2:* Given that the goal is to minimize the outage time, one would ideally like to *impose* that UAV-2 remains in the set of locations where it can provide r_{UE}^{\min} to the UE for a suitable location of UAV-1. Since this set generally changes over time and, therefore, such an approach need not be feasible, a reasonable alternative is to *encourage* UAV-2 to stay in these sets of locations by planning a path through an extended graph with properly weighted edges.

To construct such a graph, note that the set of candidate locations of UAV-2 is $\mathcal{N}_2 \triangleq \mathcal{R}(\mathbf{q}_{BS}, 2r_{CC}, r_{CC})$ and does not depend on the location of the UE. With $\tilde{\mathcal{N}}_2[n] \triangleq \{(n, \mathbf{q}) | \mathbf{q} \in \mathcal{N}_2\}$ denoting the set of extended nodes at time step n , the node set of the extended graph is $\tilde{\mathcal{N}}_2 \triangleq \cup_n \tilde{\mathcal{N}}_2[n]$. In contrast, the set of destinations $\mathcal{D}_2[n] \triangleq \mathcal{R}(\mathbf{q}_{BS}, 2r_{CC} + r_{UE}^{\min}, r_{CC} + r_{UE}^{\min}) \cap \mathcal{R}(\mathbf{q}_{UE}[n], r_{UE}^{\min})$, which comprises those locations where UAV-2 can provide r_{UE}^{\min} to the UE, does generally change over time as it depends on $\mathbf{q}_{UE}[n]$. The corresponding set of extended nodes at time step n is given by $\tilde{\mathcal{D}}_2[n] \triangleq \{(n, \mathbf{q}) | \mathbf{q} \in \mathcal{D}_2[n]\} \subset \tilde{\mathcal{N}}_2[n] \subset \tilde{\mathcal{N}}_2$.

In this graph, nodes (n, \mathbf{q}) and (n', \mathbf{q}') are connected by an edge iff $n' = n + 1$ and $(\mathbf{q}', \mathbf{q}) \in \mathcal{E}_{\bar{\mathcal{F}}_G}$. In this way, a path for UAV-2 is a sequence of extended nodes $(0, \mathbf{q}_2[0]), (1, \mathbf{q}_2[1]), \dots, (N_{UE} - 1, \mathbf{q}_2[N_{UE} - 1])$ where $(n, \mathbf{q}_2[n]) \in \tilde{\mathcal{N}}_2[n]$ and $(\mathbf{q}_2[n], \mathbf{q}_2[n + 1]) \in \mathcal{E}_{\bar{\mathcal{F}}_G} \forall n$. The weight of an edge $((n, \mathbf{q}), (n', \mathbf{q}'))$, which captures the cost of traveling from (n, \mathbf{q}) to (n', \mathbf{q}') , is given by

$$w((n, \mathbf{q}), (n', \mathbf{q}')) = \begin{cases} 0 & \text{if } \mathbf{q} = \mathbf{q}', \mathbf{q}' \in \mathcal{D}_2[n'] \\ 1 & \text{if } \mathbf{q} \neq \mathbf{q}', \mathbf{q}' \in \mathcal{D}_2[n'] \\ w_p & \text{if } \mathbf{q}' \notin \mathcal{D}_2[n'], \end{cases} \quad (16)$$

where w_p is a large positive number that encourages UAV-2 to stay in $\tilde{\mathcal{D}}_2[n]$ at time step n . Observe that, even when UAV-2 remains in these sets, the cost is greater if it moves.

A shortest path algorithm is used to find the path of UAV-2 from the extended node corresponding to the take-off location to any extended node in $\tilde{\mathcal{N}}_2[N_{UE} - 1]$. The procedure to find the path of UAV-2 is summarized as Algorithm 4.

2) *Path for UAV-1*: With the cost in (16), the number of time slots where UAV-2 is in a location that can provide r_{UE}^{\min} to the UE for a suitable location of UAV-1 is maximized. By suitable location it is meant that UAV-1 can provide $r_{\text{CC}} + r_{\text{UE}}^{\min}$ to UAV-2. Unfortunately, since the set of suitable locations for UAV-1 changes with n , it may not be possible for UAV-1 to be in a suitable location all the time. By finding a path for UAV-1 so that it stays within these sets as much as possible, the combined path will approximately minimize the outage time.

To this end, the path must be planned through an extended graph. Let $p_2 = \{\mathbf{q}_2[0], \mathbf{q}_2[1], \dots, \mathbf{q}_2[N_{\text{UE}} - 1]\}$ be the path of UAV-2 returned by Algorithm 4. The set of candidate locations of UAV-1 at time step n is $\mathcal{N}_1[n] \triangleq \mathcal{R}(\mathbf{q}_{\text{BS}}, 2r_{\text{CC}}) \cap \mathcal{R}(\mathbf{q}_2[n], r_{\text{CC}})$ and the associated set of extended nodes is $\bar{\mathcal{N}}_1[n] \triangleq \{(n, \mathbf{q}) | \mathbf{q} \in \mathcal{N}_1[n]\}$. The node set of the extended graph is therefore $\bar{\mathcal{N}}_1 \triangleq \cup_n \bar{\mathcal{N}}_1[n]$. On the other hand, the set of destinations of UAV-1 at time step n is given by $\mathcal{D}_1[n] \triangleq \mathcal{R}(\mathbf{q}_{\text{BS}}, 2r_{\text{CC}} + r_{\text{UE}}^{\min}) \cap \mathcal{R}(\mathbf{q}_2[n], r_{\text{CC}} + r_{\text{UE}}^{\min}) \subset \bar{\mathcal{N}}_1[n]$.

As opposed to Sec. V-A, UAV-2 cannot wait for UAV-1 since that would introduce an offset between a part of p_2 and p_{UE} . Nodes (n, \mathbf{q}) and (n', \mathbf{q}') are therefore connected by an edge iff $n' = n + 1$ and $(\mathbf{q}', \mathbf{q}) \in \mathcal{E}_{\bar{\mathcal{F}}_G}$. This means that the path of UAV-1 in the extended graph will have the form $(0, \mathbf{q}_1[0]), (1, \mathbf{q}_1[1]), \dots, (N_{\text{UE}} - 1, \mathbf{q}_1[N_{\text{UE}} - 1])$, where $(n, \mathbf{q}_1[n]) \in \bar{\mathcal{N}}_1[n]$ and $(\mathbf{q}_1[n], \mathbf{q}_1[n+1]) \in \mathcal{E}_{\bar{\mathcal{F}}_G} \forall n$. Similarly to UAV-2, the weight of the edge from (n, \mathbf{q}) to (n', \mathbf{q}') is given by (16) with $\mathcal{D}_1[n']$ in place of $\mathcal{D}_2[n']$.

The goal is, therefore, to find a path from the extended node corresponding to the take-off location to any node in $\bar{\mathcal{N}}_1[N_{\text{UE}} - 1]$. Among such feasible paths, a shortest path algorithm picks the one that results in the lowest accumulated cost, hence the lowest outage time if w_p is sufficiently large.

Lifting. As in Sec. V, given p_2 there may be no path for UAV-1 such that the combined path is feasible. Similarly to Sec. V-A2, one can remedy this by lifting p_2 since this generally expands the sets of candidate locations of UAV-1. However, the lifting operator to be used here differs from the one in Sec. V-A2 since it must preserve the path length.

Consider an arbitrary path $p = \{\mathbf{q}[0], \mathbf{q}[1], \dots, \mathbf{q}[N - 1]\}$. Let $A(p) \triangleq \{\mathbf{q}[0], L(\mathbf{q}[0]), L(\mathbf{q}[1]), \dots, L(\mathbf{q}[N - 1])\}$, where L is defined in (12), be an operator that lifts each point and appends the first one at the beginning. Observe that the length of $A(p)$ equals the length of p plus 1. Also, let $A^{(1)}(p) \triangleq A(p)$ and $A^{(u)}(p) \triangleq A(A^{(u-1)}(p))$. On the other hand, let $Z(p) \triangleq \{\mathbf{q}[0], \mathbf{q}[1], \dots, \mathbf{q}[\bar{n} - 1], \mathbf{q}[\bar{n} + 1], \dots, \mathbf{q}[N - 1]\}$, where \bar{n} is the smallest n such that $\mathbf{q}[n] = \mathbf{q}[n + 1]$ and $\bar{n} = N - 1$ if $\mathbf{q}[n] \neq \mathbf{q}[n + 1]$ for all n . Observe that the length of $Z(p)$ equals the length of p minus 1. Also, $Z^{(1)}(p) \triangleq Z(p)$ and $Z^{(i)}(p) \triangleq Z(Z^{(i-1)}(p))$. Finally, let $\bar{L}^{(0)}(p) = p$ and let $\bar{L}^{(u)}(p) \triangleq Z^{(u)}(A^{(u)}(p))$ for $u > 0$. Note that (i) the length of $\bar{L}^{(u)}(p)$ equals the length of p , and (ii), if p is a path where each pair of consecutive waypoints are adjacent in \mathcal{G} , the same holds for $\bar{L}^{(u)}(p)$.

As in Sec. V-A2, the lifting operator is iteratively applied to p_2 until a path $\{\mathbf{q}_1[0], \mathbf{q}_1[1], \dots, \mathbf{q}_1[N_{\text{UE}} - 1]\}$ for UAV-1 is found. With u the number of required lifting steps, the tentative path is then $P^{\text{F}} = \{\mathbf{Q}[0], \dots, \mathbf{Q}[N_{\text{UE}} - 1]\}$, where $\mathbf{Q}[n] = [\mathbf{q}_1[n], \hat{\mathbf{q}}_2[n]]$ for $\{\hat{\mathbf{q}}_2[0], \dots, \hat{\mathbf{q}}_2[N_{\text{UE}} - 1]\} \triangleq \bar{L}^{(u)}(p_2)$. This

procedure is summarized as Algorithm 5.

3) *Theoretical Guarantees*: As in Sec. V-A3, it is possible to guarantee that the above iterative lifting procedure will eventually produce a feasible path.

Let h_{max} be the height of the lowest grid level that is higher than all obstacles and let $\bar{\mathcal{F}}_G^{\text{max}} \triangleq \{\mathbf{q} \in \bar{\mathcal{F}}_G : [0, 0, 1] \mathbf{q} = h_{\text{max}}\}$ be the grid level of height h_{max} . Let $\mathcal{C}(d_{\text{C}}) \triangleq \{[x, y, z]^{\text{T}} \in \mathbb{R}^3 : (x - x_{\text{BS}})^2 + (y - y_{\text{BS}})^2 \leq d_{\text{C}}^2\}$ be a cylinder of radius d_{C} centered at \mathbf{q}_{BS} and let $d_{\text{C}, \text{min}}$ be the smallest d_{C} such that $\bar{\mathcal{F}}_G \subset \mathcal{C}(d_{\text{C}})$ or, equivalently, the maximum horizontal distance from the BS to any point in $\bar{\mathcal{F}}_G$.

Theorem 2: Suppose that $\mathbf{Q}_0 = [\mathbf{q}_{\text{BS}}, \mathbf{q}_{\text{BS}}]$ and let p_2 be the path of UAV-2 returned by Algorithm 4. If $h_{\text{max}} \leq \bar{c}^{-1}(2r_{\text{CC}})$ and $d_{\text{C}, \text{min}} \leq \bar{c}^{-1}(r_{\text{CC}})$, then Algorithm 5 will provide a feasible combined path.

Proof: See Appendix D. ■

It is also easy to see that, for a sufficiently large w_p , the tentative path is not only feasible but also optimal in terms of outage time if no lifting steps are required and UAV-1 remains at destination points throughout the entire path. When it comes to total transferred data, the tentative path will not generally be optimal, but can reasonably be expected to be similar to the optimal path in many cases.

B. Probabilistic Roadmaps with Feasible Initialization

The next step is to find a combined path around the tentative path that approximately optimizes the considered metric. Since the set of candidate CPs changes over time, an extended graph needs to be adopted. To operate on this graph, the PR algorithm in Sec. IV will be generalized.

1) *Construction of the Node Set*: In addition to the CPs in the tentative path $P^{\text{F}} = \{\mathbf{Q}[0], \dots, \mathbf{Q}[N_{\text{UE}} - 1]\}$, the algorithm draws $C \geq N_{\text{UE}}$ additional CPs. In particular, $\lfloor C/N_{\text{UE}} \rfloor$ CPs are drawn around each $\mathbf{Q}[n]$ as in Sec. V-B1. With $\mathcal{N}[n]$ representing the set that contains $\mathbf{Q}[n]$ and the CPs drawn around $\mathbf{Q}[n]$, the set of extended nodes at time step n is given by $\bar{\mathcal{N}}[n] \triangleq \{(n, \mathbf{Q}) | \mathbf{Q} \in \mathcal{N}[n]\}$.

2) *Construction of the Edge Set*: Two extended nodes (n, \mathbf{Q}) and (n', \mathbf{Q}') are connected by an edge iff $n' = n + 1$, $(\mathbf{q}_1, \mathbf{q}'_1) \in \mathcal{E}_{\bar{\mathcal{F}}_G}$, and $(\mathbf{q}_2, \mathbf{q}'_2) \in \mathcal{E}_{\bar{\mathcal{F}}_G}$, where $\mathbf{Q} = [\mathbf{q}_1, \mathbf{q}_2]$ and $\mathbf{Q}' = [\mathbf{q}'_1, \mathbf{q}'_2]$. The edge weights depend on the metric to be optimized. To minimize the outage time, one needs to minimize the number of time slots in which $r_{\text{UE}}(\mathbf{Q}[n], \mathbf{q}_{\text{UE}}[n])$ is below r_{UE}^{\min} (this follows by discretizing (10) as $J(\mathbf{Q}(\cdot)) \approx \tau \sum_0^{N-1} \mathcal{I}[r_{\text{UE}}(\mathbf{Q}[n], \mathbf{q}_{\text{UE}}[n]) < r_{\text{UE}}^{\min}]$). As a result, one can set

$$w((n, \mathbf{Q}), (n', \mathbf{Q}')) = \begin{cases} 0 & \text{if } \mathbf{Q} = \mathbf{Q}', r_{\text{UE}}(\mathbf{Q}') \geq r_{\text{UE}}^{\min} \\ 1 & \text{if } \mathbf{Q} \neq \mathbf{Q}', r_{\text{UE}}(\mathbf{Q}') \geq r_{\text{UE}}^{\min} \\ w_p & \text{if } r_{\text{UE}}(\mathbf{Q}') < r_{\text{UE}}^{\min}, \end{cases} \quad (17)$$

where w_p is again a large positive number. To maximize the transferred data, observe that the integral in (11) can be discretized as

$$J(\mathbf{Q}(\cdot)) \approx -\tau \sum_{n=0}^{N_{\text{UE}}-1} r_{\text{UE}}(\mathbf{Q}[n], \mathbf{q}_{\text{UE}}[n]). \quad (18)$$

Algorithm 4: Tentative Path UAV-2, Moving UE

input: $\bar{\mathcal{F}}_G, \mathbf{q}_{BS}, \mathbf{q}_2[0]$,
 $p_{UE} =$
 $\{\mathbf{q}_{UE}[0], \mathbf{q}_{UE}[1], \dots, \mathbf{q}_{UE}[N_{UE} - 1]\}, r_{CC}, r_{UE}^{\min}, c$

- 1: Find the candidate locations of UAV-2
 $\rightarrow \mathcal{N}_2[n] = \mathcal{R}(\mathbf{q}_{BS}, 2r_{CC}, r_{CC})$
- 2: Find the destinations of UAV-2 $\rightarrow \mathcal{D}_2[n] =$
 $\mathcal{R}(\mathbf{q}_{BS}, 2r_{CC} + r_{UE}^{\min}, r_{CC} + r_{UE}^{\min}) \cap \mathcal{R}(\mathbf{q}_{UE}[n], r_{UE}^{\min})$
- 3: Construct extended graph \mathcal{G}_3 with weights (16)
- 4: $p_2 \triangleq \text{shortest_path}((0, \mathbf{q}_2[0]), \mathcal{N}_2[N_{UE} - 1])$
- 5: **return** $p_2 = \{\mathbf{q}_2[0], \mathbf{q}_2[1], \dots, \mathbf{q}_2[N_{UE} - 1]\}$

Since a shortest path algorithm minimizes the sum of the weights of the edges in a path, one can therefore set $w((n, \mathbf{Q}), (n', \mathbf{Q}')) = -r_{UE}(\mathbf{Q}', \mathbf{q}_{UE}[n'])^3$.

3) *Path Planning in Q-Space:* A shortest-path algorithm is then used to find the path $P^{\text{PR}} = \{\mathbf{Q}[0], \mathbf{Q}[1], \dots, \mathbf{Q}[N_{UE} - 1]\}$ of the UAVs in the extended graph from \mathbf{Q}_0 to an extended node in $\mathcal{N}[N_{UE} - 1]$ that results in the lowest accumulated cost. This differs from standard PR, which finds a shortest path through a nearest-neighbor graph.

C. From the Waypoint Sequence to the Trajectory

As described at the beginning of Sec. VI, the produced path for the UAVs is sampled at regular intervals τ . Thus, given P^{PR} , the final trajectory $\mathbf{Q}(\cdot)$ satisfies $\mathbf{Q}(n\tau) = \mathbf{Q}[n], n = 0, \dots, N_{UE} - 1$. As indicated earlier, the position of the UAVs at intermediate time instants is determined by the flight controller. Observe that PRFI for moving UEs returns a path in which the UAVs fly to adjacent grid points at each time step, albeit not necessarily at maximum speed. Meanwhile, PRFI for static UEs returns a path in which the UAVs fly at their maximum speed from $\mathbf{Q}[n]$ to $\mathbf{Q}[n + 1]$, but, $\mathbf{q}_k[n]$ is not necessarily adjacent to $\mathbf{q}_k[n + 1]$ on the grid. Therefore, although PRFI for moving UEs can be used to serve static UEs, PRFI for static UEs generally has greater optimality.

The complete procedure is summarized as Algorithm 6; see Secs. VII-A, VII-B and VII-C for generalizations and complexity analysis.

Since τ affects the optimality of the obtained trajectory, it is important to set it as low as allowed by the available computational resources. To this end, note that the complexity of the algorithm can be expressed as a function $f(N_{UE}, N_{\text{grid}})$. It can be shown that f is $\mathcal{O}(N_{UE} N_{\text{grid}} \log(N_{UE} N_{\text{grid}}))$ (cf. Sec. VII-C) in order notation, but the exact expression, which depends on the implementation, is required here. The idea is to express N_{UE} and N_{grid} in terms of τ and then solve for τ . Specifically, start by noting that $N_{UE} = T/\tau$. On the other hand, note that τ should equal the time a UAV needs to fly to the farthest adjacent grid point at full speed. If, for simplicity, \mathcal{F} is a cube of side length L and $\delta \triangleq \delta_x = \delta_y = \delta_z$, then $\tau = \sqrt{3}\delta/v_{\max} = \sqrt{3}L/(v_{\max} \sqrt[3]{N_{\text{grid}}})$. This implies that $N_{\text{grid}} = [\sqrt{3}L/(\tau v_{\max})]^3$.

³Indeed, other additive (cumulative) metrics (objectives) can also be optimized by the same approach.

Algorithm 5: Tentative Path UAV-1, Moving UE

input: $\bar{\mathcal{F}}_G, \mathbf{q}_{BS}, \mathbf{q}_1[0], p_2, r_{CC}, r_{UE}^{\min}, c$

- 1: **for** $u = 0, 1, \dots$ **do**
- 2: $\{\hat{\mathbf{q}}_2[0], \hat{\mathbf{q}}_2[1], \dots, \hat{\mathbf{q}}_2[N_{UE} - 1]\} \triangleq \bar{L}^{(u)}(p_2)$
- 3: Find the candidate locations of UAV-1
 $\rightarrow \mathcal{N}_1[n] = \mathcal{R}(\mathbf{q}_{BS}, 2r_{CC}) \cap \mathcal{R}(\hat{\mathbf{q}}_2[n], r_{CC})$
- 4: Find the destinations of UAV-1
 $\rightarrow \mathcal{D}_1[n] = \mathcal{R}(\mathbf{q}_{BS}, 2r_{CC} + r_{UE}^{\min}) \cap \mathcal{R}(\hat{\mathbf{q}}_2[n], r_{CC} + r_{UE}^{\min})$
- 5: Form extended nodes $\rightarrow \tilde{\mathcal{N}}_1[n] \triangleq \{(n, \mathbf{q}) | \mathbf{q} \in \mathcal{N}_1[n]\}$
- 6: Construct extended graph \mathcal{G}_4 with weights given in Sec. VI-A2.
- 7: **if** $\text{path_exists}((0, \mathbf{q}_1[0]), \tilde{\mathcal{N}}_1[N_{UE} - 1])$ **then**
- 8: $\{(0, \mathbf{q}_1[0]), \dots, (N_{UE} - 1, \mathbf{q}_1[N_{UE} - 1])\}$
 $= \text{shortest_path}((0, \mathbf{q}_1[0]), \tilde{\mathcal{N}}_1[N_{UE} - 1])$
- 9: Obtain $\mathbf{Q}[n] = [\mathbf{q}_1[n], \hat{\mathbf{q}}_2[n]]$, $n = 0, 1, \dots, N_{UE} - 1$
- 10: **Return** $P^{\text{F}} = \{\mathbf{Q}[0], \mathbf{Q}[1], \dots, \mathbf{Q}[N_{UE} - 1]\}$
- 11: **end if**
- 12: **end for**

Algorithm 6: PRFI for Moving UE

input: $\bar{\mathcal{F}}_G, \mathbf{q}_{BS}, \mathbf{Q}_0, p_{UE}, C, \tau, r_{CC}, r_{UE}^{\min}, c$

- 1: $p_2 \triangleq$ tentative path for UAV-2 via Algorithm 4
- 2: $P^{\text{F}} \triangleq$ combined tentative path via Algorithm 5
- 3: For each $\mathbf{Q}[n] \in P^{\text{F}}$, draw $\lfloor C/N_{UE} \rfloor$ CPs $\rightarrow \mathcal{N}[n]$
- 4: Construct extended graph with weights as in Sec. VI-B
- 5: $P^{\text{PR}} \triangleq \text{shortest_path}((0, \mathbf{Q}_0), \mathcal{N}[N_{UE} - 1])$
- 6: **return** times and waypoints $\{(n\tau, \mathbf{Q}[n])\}_n$.

As a result, the complexity can be written as $f(T/\tau, [\sqrt{3}L/(\tau v_{\max})]^3)$. Equating this expression to the available resources and solving for τ yields the desired τ (and also δ as $\delta = v_{\max}\tau/\sqrt{3}$).

VII. EXTENSIONS

A. Extension to more than two UAVs

This section extends Algorithms 3 and 6 to the case of more than two UAVs. To this end, let $\mathcal{R}(\mathbf{q}, r_1, r_2, \dots, r_k) \triangleq \{\mathbf{q}' \in \bar{\mathcal{F}}_G | \exists \bar{\mathbf{q}} \in \mathcal{R}(\mathbf{q}, r_1, r_2, \dots, r_{k-1}) : c(\bar{\mathbf{q}}, \mathbf{q}') \geq r_k\}$, $k > 2$. PRFI for static UEs is extended to K UAVs, $K > 2$, as follows. The tentative path of UAV- K is planned by Algorithm 1 after replacing \mathcal{N}_2 and \mathcal{D}_2 in Steps 1 and 2 with $\mathcal{N}_K \triangleq \mathcal{R}(\mathbf{q}_{BS}, Kr_{CC}, (K-1)r_{CC}, \dots, 2r_{CC}, r_{CC})$ and $\mathcal{D}_K \triangleq \mathcal{R}(\mathbf{q}_{BS}, Kr_{CC} + r_{UE}^{\min}, (K-1)r_{CC} + r_{UE}^{\min}, \dots, 2r_{CC} + r_{UE}^{\min}, r_{CC} + r_{UE}^{\min}) \cap \mathcal{R}(\mathbf{q}_{UE}, r_{UE}^{\min})$. The tentative path of UAV- k , $k = K-1, K-2, \dots, 1$, is planned by Algorithm 2 after replacing $\mathcal{N}_1[n]$ and $\mathcal{D}_1[n]$ in Steps 3 and 4 with $\mathcal{N}_k[n] = \mathcal{R}(\mathbf{q}_{BS}, Kr_{CC}, (K-1)r_{CC}, \dots, (K-k+1)r_{CC}) \cap \mathcal{R}(\hat{\mathbf{q}}_{k+1}[n], (K-k)r_{CC})$ and $\mathcal{D}_k[n] = \mathcal{R}(\mathbf{q}_{BS}, Kr_{CC} + r_{UE}^{\min}, (K-1)r_{CC} + r_{UE}^{\min}, \dots, (K-k+1)r_{CC} + r_{UE}^{\min}) \cap \mathcal{R}(\hat{\mathbf{q}}_{k+1}[n], (K-k)r_{CC} + r_{UE}^{\min})$. In Step 2, the path of UAV- k' needs to be lifted for all $k' > k$. The remaining steps can be readily extended. By planning the tentative path for the K UAVs in this way, Algorithm 3 is extended to find the approximately optimal path. In the extension above, Algorithm 2

adopts the waiting approach (described in Sec. V-A2) to plan the tentative path for UAV- k . This approach may require UAV- $(k+1)$ to wait at some time steps. This then requires UAV- $(k+2)$ to wait for UAV- $(k+1)$, UAV- $(k+3)$ to wait for UAV- $(k+2)$, and so on.

Similarly, PRFI for moving UEs can be extended to $K > 2$ by successively planning the tentative path for UAV- K , then UAV- $(K-1)$ and so on. Particularly, the tentative path of UAV- K is planned by Algorithm 4 after replacing $\mathcal{N}_2[n]$ and $\mathcal{D}_2[n]$ in Steps 1 and 2 with $\mathcal{N}_K[n] \triangleq \mathcal{R}(\mathbf{q}_{\text{BS}}, Kr_{\text{CC}}, (K-1)r_{\text{CC}}, \dots, 2r_{\text{CC}}, r_{\text{CC}})$ and $\mathcal{D}_K[n] \triangleq \mathcal{R}(\mathbf{q}_{\text{BS}}, Kr_{\text{CC}} + r_{\text{UE}}^{\min}, (K-1)r_{\text{CC}} + r_{\text{UE}}^{\min}, \dots, 2r_{\text{CC}} + r_{\text{UE}}^{\min}, r_{\text{CC}} + r_{\text{UE}}^{\min}) \cap \mathcal{R}(\mathbf{q}_{\text{UE}}[n], r_{\text{UE}}^{\min})$. The tentative path of UAV- k , $k = K-1, K-2, \dots, 1$, is planned by Algorithm 5 after replacing $\mathcal{N}_1[n]$ and $\mathcal{D}_1[n]$ in Steps 3 and 4 with $\mathcal{N}_k[n] = \mathcal{R}(\mathbf{q}_{\text{BS}}, Kr_{\text{CC}}, (K-1)r_{\text{CC}}, \dots, (K-k+1)r_{\text{CC}}) \cap \mathcal{R}(\hat{\mathbf{q}}_{k+1}[n], (K-k)r_{\text{CC}})$ and $\mathcal{D}_k[n] = \mathcal{R}(\mathbf{q}_{\text{BS}}, Kr_{\text{CC}} + r_{\text{UE}}^{\min}, (K-1)r_{\text{CC}} + r_{\text{UE}}^{\min}, \dots, (K-k+1)r_{\text{CC}} + r_{\text{UE}}^{\min}) \cap \mathcal{R}(\hat{\mathbf{q}}_{k+1}[n], (K-k)r_{\text{CC}} + r_{\text{UE}}^{\min})$. In Step 2, the path of UAV- k' needs to be lifted for $k' > k$. The remaining steps can be readily extended. By planning the tentative paths of the K UAVs, Algorithm 6 is extended to find the approximately optimal path.

B. Extension to multiple UEs

This section extends Algorithms 3 and 6 to the case of multiple UEs. Extending the algorithms in Sec. VII-A follows along the same lines. Let M and $\{1, 2, \dots, M\}$ respectively denote the number and the set of indices of the UEs.

In the case of static UEs, the location of the m -th UE is denoted by $\mathbf{q}_{\text{UE}}^{(m)}$. Given a configuration point \mathbf{Q} , the achievable rate of the m -th UE is $r_{\text{UE}}^{(m)}(\mathbf{Q}) \triangleq r_{\text{UE}}(\mathbf{Q}, \mathbf{q}_{\text{UE}}^{(m)})$. For simplicity, assume that each UE requires the same rate r_{UE}^{\min} . Since it may not be possible to serve all UEs at the same time, a reasonable objective would be to serve as many UEs as possible. Formally, the index set \mathcal{M} of served UEs can be taken to be the largest subset of $\{1, 2, \dots, M\}$ such that the destination set $\tilde{\mathcal{D}}^{\text{UE}} \triangleq \cap_{m \in \mathcal{M}} \mathcal{R}(\mathbf{q}_{\text{UE}}^{(m)}, r_{\text{UE}}^{\min})$ is not empty. Then, Algorithms 1 and 2 are modified as follows: $\{\mathbf{q}_{\text{UE}}^{(m)}\}_{m \in \tilde{\mathcal{D}}^{\text{UE}}}$ will be one of the inputs. \mathcal{D}_2 in Step 2 in Algorithm 1 is replaced with $\mathcal{D}_2 = \mathcal{R}(\mathbf{q}_{\text{BS}}, 2r_{\text{CC}} + |\mathcal{M}|r_{\text{UE}}^{\min}, r_{\text{CC}} + |\mathcal{M}|r_{\text{UE}}^{\min}) \cap \tilde{\mathcal{D}}^{\text{UE}}$. \mathcal{D}_1 in Step 4 of Algorithm 2 is then replaced with $\mathcal{D}_1 = \mathcal{R}(\mathbf{q}_{\text{BS}}, 2r_{\text{CC}} + |\mathcal{M}|r_{\text{UE}}^{\min}) \cap \mathcal{R}(\hat{\mathbf{q}}_2[N_u - 1], r_{\text{CC}} + |\mathcal{M}|r_{\text{UE}}^{\min})$. Finally, Algorithm 3 is used to find the approximately optimal path by replacing Step 5 with $P^{\text{PR}} := \text{shortest_path}(\mathbf{Q}_0, \{\mathbf{Q} \in \mathcal{N} : r_{\text{UE}}^{(m)}(\mathbf{Q}) \geq r_{\text{UE}}^{\min}, \forall m \in \mathcal{M}\})$.

In the case of moving UEs, assume without loss of generality that all UEs follow paths of length N_{UE} . The trajectory of the m -th UE can then be denoted by $\mathcal{P}_{\text{UE}}^{(m)} \triangleq \{\mathbf{q}_{\text{UE}}^{(m)}[0], \mathbf{q}_{\text{UE}}^{(m)}[1], \dots, \mathbf{q}_{\text{UE}}^{(m)}[N_{\text{UE}} - 1]\}$, where $\mathbf{q}_{\text{UE}}^{(m)}[n]$ is the location of the m -th UE at time step n . Since it may not be possible to provide connectivity to all UEs at every time step, a reasonable objective would be to serve as many UEs as possible. Formally, the index set $\mathcal{M}[n]$ of served UEs at time step n can be taken to be the largest subset of $\{1, 2, \dots, M\}$ such that $\tilde{\mathcal{D}}^{\text{UE}}[n] \triangleq \cap_{m \in \mathcal{M}[n]} \mathcal{R}(\mathbf{q}_{\text{UE}}^{(m)}[n], r_{\text{UE}}^{\min}) \neq \emptyset$. Then, Algorithms 4 and 5 are modified as follows. $\{\mathcal{P}_{\text{UE}}^{(m)}\}_{m=1}^M$

will be one of the inputs. $\mathcal{D}_2[n]$ in Step 2 of Algorithm 4 is replaced with $\mathcal{D}_2[n] = \mathcal{R}(\mathbf{q}_{\text{BS}}, 2r_{\text{CC}} + |\mathcal{M}[n]|r_{\text{UE}}^{\min}, r_{\text{CC}} + |\mathcal{M}[n]|r_{\text{UE}}^{\min}) \cap \tilde{\mathcal{D}}^{\text{UE}}[n]$. $\mathcal{D}_1[n]$ in Step 4 of Algorithm 5 is replaced with $\mathcal{D}_1[n] = \mathcal{R}(\mathbf{q}_{\text{BS}}, 2r_{\text{CC}} + |\mathcal{M}[n]|r_{\text{UE}}^{\min}) \cap \mathcal{R}(\hat{\mathbf{q}}_2[n], r_{\text{CC}} + |\mathcal{M}[n]|r_{\text{UE}}^{\min})$. These modifications extend Algorithm 6 to the case $M > 1$.

C. Complexity analysis

Assume for simplicity that $M = 1$, \mathcal{F} is a cube of side L , and $\delta_x = \delta_y = \delta_z = \delta > 0$. The number of grid points is then roughly $N_{\text{grid}} = L^3/\delta^3$, which implies that $\delta = L/\sqrt[3]{N_{\text{grid}}}$. Overall, the proposed algorithms utilize $\mathcal{N}_k[n]$ and $\mathcal{D}_k[n]$; cf. Sec. VII-A. This requires $\tilde{\mathcal{N}}_k \triangleq \mathcal{R}(\mathbf{q}_{\text{BS}}, Kr_{\text{CC}}, (K-1)r_{\text{CC}}, \dots, (K-k+1)r_{\text{CC}})$ and $\tilde{\mathcal{D}}_k \triangleq \mathcal{R}(\mathbf{q}_{\text{BS}}, Kr_{\text{CC}} + r_{\text{UE}}^{\min}, (K-1)r_{\text{CC}} + r_{\text{UE}}^{\min}, \dots, (K-k+1)r_{\text{CC}} + r_{\text{UE}}^{\min}), \forall k = 1, \dots, K$. Obtaining these sets does not count towards complexity as it only requires comparisons – the capacity map c already provides $c(\mathbf{q}, \mathbf{q}')$ for all $\mathbf{q}, \mathbf{q}' \in \bar{\mathcal{F}}_{\text{G}}$. Therefore, the complexity of the proposed algorithms mainly stems from the adopted shortest path algorithm. In the case of Dijkstra's, its standard implementation has complexity $\mathcal{O}((V+E)\log V)$ [15], where V and E are the numbers of vertices and edges of the considered graph. Based on this, the complexity of the proposed algorithms is obtained next.

Start by considering the case of a static UE. The first step is to obtain the complexity of computing the tentative path. Suppose initially that $K = 2$. Planning the path of UAV-2 involves N_{grid} nodes and $26N_{\text{grid}}/2$ edges, which requires $\mathcal{O}((N_{\text{grid}} + 13N_{\text{grid}})\log(N_{\text{grid}})) = \mathcal{O}(N_{\text{grid}}\log(N_{\text{grid}}))$ operations. If this path has N nodes, planning the path of UAV-1 involves an extended graph with NN_{grid} nodes and $27NN_{\text{grid}}$ edges. This requires $\mathcal{O}((NN_{\text{grid}} + 27NN_{\text{grid}})\log(NN_{\text{grid}})) = \mathcal{O}(NN_{\text{grid}}\log(NN_{\text{grid}}))$ operations. Proceeding along these lines for $K > 2$ yields

$$\mathcal{O}(KNN_{\text{grid}}\log(NN_{\text{grid}})). \quad (19)$$

Planning the combined path involves C nodes and $CN_{\text{nb}}/2$ edges, where N_{nb} is the number of neighbors of a node. Since these are constants, the contribution of this step to the overall complexity can be neglected. Thus, in short, the complexity of PRFI for static UEs is given by (19).

This complexity can be related to existing schemes. To this end, note that:

- the complexity of [30] and [14] is $\mathcal{O}(KN^{3.5}\log(1/\epsilon))$, where $\epsilon = 10^{-3}$ is the solution accuracy.
- [31] has complexity $\mathcal{O}(U(KN)^{3.5})$, where U is the number of iterations.
- the complexity of [29] is only said to be polynomial w.r.t N , but it is likely larger than (19).
- obtaining an exact solution in [8], [13] is NP-hard (although polynomial time approximations can be used).

Thus, the complexity of existing schemes in terms of N typically grows as $\mathcal{O}(N^{3.5})$, much faster than with the proposed algorithm, for which complexity grows as $\mathcal{O}(N\log(N))$.

Next, consider the case of a moving UE. First, the computation of the tentative path will be considered. For planning the path of UAV- K , one needs $\mathcal{N}_K[n] = \tilde{\mathcal{N}}_K$, which is already

TABLE II: Simulation parameters unless otherwise stated.

Notation	Physical meaning	Simulation value
$S \in \mathbb{R}^3$	Considered region [m×m×m]	$500 \times 500 \times 100$
\mathcal{F}_G	Flight grid [$N_x^{\text{grid}} \times N_y^{\text{grid}} \times N_z^{\text{grid}}$]	$12 \times 12 \times 8$
	Minimum flight height	12.5 m
h_{top}	Maximum flight height	87.5 m
\mathbf{q}_{BS}	Location of the BS	$[20, 470, 0]^T$
	Number of buildings	25
K	Number of UAVs	2
v_{max}	Maximum UAV speed	7 m/s
r_{CC}	Minimum UAV rate	200 kbps
	Carrier frequency	6 GHz
B	Bandwidth	20 MHz
P_t	Transmit power	17 dBm
G_t, G_r	Tx./Rx. Antenna gain	12 dBi
σ^2	Noise power	-97 dBm
C	No. of configuration points in PRFI	2000
	No. of neighbors in PRFI	100
	No. of Monte Carlo (MC) realizations	400

known. One also needs $\mathcal{D}_K[n] = \tilde{\mathcal{D}}_K \cap \mathcal{R}(\mathbf{q}_{\text{UE}}[n], r_{\text{UE}}^{\min})$, which in turn requires computing $\mathcal{R}(\mathbf{q}_{\text{UE}}[n], r_{\text{UE}}^{\min})$. Since this involves N_{grid} operations, finding $\mathcal{D}_K[n] \forall n$ has complexity $N_{\text{UE}} N_{\text{grid}}$. Having obtained $\mathcal{N}_K[n]$ and $\mathcal{D}_K[n]$, the next step is to plan the path of UAV- K through an extended graph with $N_{\text{UE}} N_{\text{grid}}$ nodes and $13 N_{\text{UE}} N_{\text{grid}}$ edges, which has complexity $\mathcal{O}((N_{\text{UE}} N_{\text{grid}} + 13 N_{\text{UE}} N_{\text{grid}}) \log(N_{\text{UE}} N_{\text{grid}})) = \mathcal{O}(N_{\text{UE}} N_{\text{grid}} \log(N_{\text{UE}} N_{\text{grid}}))$. When planning the paths of the remaining UAVs, one must compute $\mathcal{N}_k[n]$ and $\mathcal{D}_k[n]$, $\forall n$, which only requires comparisons. After that, planning the path of UAV- k has the same complexity as planning the path of UAV- K , i.e. $\mathcal{O}(N_{\text{UE}} N_{\text{grid}} \log(N_{\text{UE}} N_{\text{grid}}))$. To sum up, the complexity of planning the tentative path is $\mathcal{O}(N_{\text{UE}} N_{\text{grid}} + K N_{\text{UE}} N_{\text{grid}} \log(N_{\text{UE}} N_{\text{grid}})) = \mathcal{O}(K N_{\text{UE}} N_{\text{grid}} \log(N_{\text{UE}} N_{\text{grid}}))$. Planning the combined path involves $\tilde{C} \triangleq \lceil C/N_{\text{UE}} \rceil + 1$ nodes and $\tilde{C}\tilde{C} = \tilde{C}^2$ edges per time step, which results in a complexity of $\mathcal{O}((\tilde{C} N_{\text{UE}} + \tilde{C}^2(N_{\text{UE}} - 1)) \log(\tilde{C} N_{\text{UE}})) = \mathcal{O}(N_{\text{UE}} \log(N_{\text{UE}}))$. Thus, the total complexity is

$$\mathcal{O}(K N_{\text{UE}} N_{\text{grid}} \log(N_{\text{UE}} N_{\text{grid}})). \quad (20)$$

Unlike the static UE case, the complexity in (20) cannot be compared with the literature since there is only one scheme for serving moving users [26] and it has no complexity analysis.

VIII. NUMERICAL EXPERIMENTS

This section presents numerical results that validate and assess the performance of the proposed algorithms. The developed simulator, the simulation code, and some videos can be found at https://github.com/uiano/pr_for_relay_path_planning.

A. Simulation Setup

Unless stated otherwise, the experiments adopt the parameters in Table II. Also, c is obtained with the tomographic channel model (cf. Sec. III-B) with an absorption of 1 dB/m inside the buildings and 0 dB/m outside.

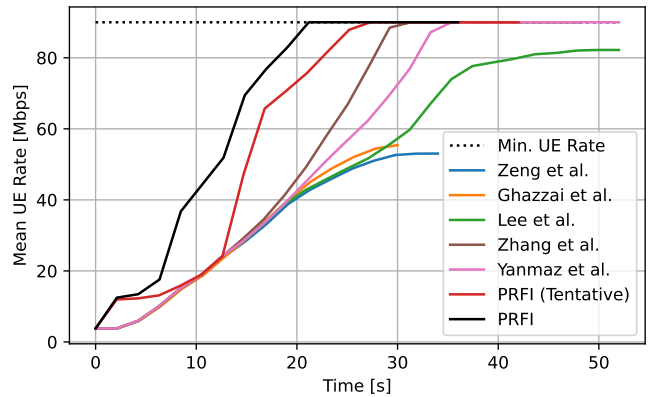


Fig. 3: Expected UE rate $\mathbb{E}[r_{\text{UE}}(\mathbf{Q}(t))]$ vs. t . The proposed algorithm is the first to attain the target rate r_{UE}^{\min} ($r_{\text{UE}}^{\min} = 90$ Mbps, $[\check{d}_{\text{BS}}^{\text{UE}}, \hat{d}_{\text{BS}}^{\text{UE}}] = [150, 250]$ m).

B. Static UE

This section studies the performance of the proposed PRFI algorithm for static UEs. Throughout this section, all buildings have a height of 40 m. For generating \mathbf{q}_{UE} at each Monte Carlo (MC) realization, the distance $d_{\text{BS}}^{\text{UE}} = \|\mathbf{q}_{\text{UE}} - \mathbf{q}_{\text{BS}}\|$ is first generated uniformly at random in the interval $[\check{d}_{\text{BS}}^{\text{UE}}, \hat{d}_{\text{BS}}^{\text{UE}}]$, where, unless otherwise stated, $\check{d}_{\text{BS}}^{\text{UE}} = 50$ m and $\hat{d}_{\text{BS}}^{\text{UE}} = 650$ m. Subsequently, \mathbf{q}_{UE} is drawn uniformly at random among the points that (i) are outside the buildings, (ii) are at a distance $d_{\text{BS}}^{\text{UE}}$ from \mathbf{q}_{BS} , and (iii) satisfy $c(\mathbf{q}_{\text{BS}}, \mathbf{q}_{\text{UE}}) \leq r_{\text{UE}}^{\min}$.

As benchmarks, this section adapts five state-of-the-art algorithms. The optimization problems that they rely on can be solved for the setup at hand, resulting in the following trajectories:

- Zeng et al. [29]: a UAV takes off vertically at the BS until reaching $\mathbf{p}_{\text{BS}}^{\text{top}} \triangleq [x_{\text{BS}}, y_{\text{BS}}, h_{\text{top}}]^T$. It then flies horizontally to $\mathbf{p}_{\text{mid}} \triangleq (\mathbf{p}_{\text{BS}}^{\text{top}} + \mathbf{p}_{\text{UE}}^{\text{top}})/2$, where $\mathbf{p}_{\text{UE}}^{\text{top}} \triangleq [x_{\text{UE}}, y_{\text{UE}}, h_{\text{top}}]^T$. This would coincide with the trajectory obtained via [30] and [14].
- Ghazzai et al. [8]: a UAV takes off at the BS to $\mathbf{p}_{\text{BS}}^{\text{top}}$ and flies horizontally to the grid point that maximizes the UE rate predicted by the channel model proposed in [1].
- Lee et al. [13]: two UAVs lift off at the BS to $\mathbf{p}_{\text{BS}}^{\text{top}}$. Then, UAV-1 flies horizontally to \mathbf{p}_{mid} . Meanwhile, UAV-2 flies horizontally to $\mathbf{p}_{\text{UE}}^{\text{top}}$.
- Zhang et al. [31]: two UAVs lift off at the BS to $\mathbf{p}_{\text{BS}}^{\text{top}}$. Then, UAV-1 stays at $\mathbf{p}_{\text{BS}}^{\text{top}}$. Meanwhile, UAV-2 flies horizontally to the grid point that maximizes the UE rate.
- Yanmaz et al. [26]: two UAVs lift off at the BS to $\mathbf{p}_{\text{BS}}^{\text{top}}$. Then, UAV-1 stays at $\mathbf{p}_{\text{BS}}^{\text{top}}$. Meanwhile, UAV-2 flies horizontally to $\mathbf{p}_{\text{UE}}^{\text{top}}$.

These algorithms are compared with PRFI (Tentative) and PRFI, which respectively correspond to Algorithms 2 and 3.

Fig. 3 compares the mean instantaneous rate $\mathbb{E}[r_{\text{UE}}(\mathbf{Q}(t))]$ of the considered algorithms. Since all UAVs start from the BS, the initial rate is the same for all algorithms. Although Zeng et al., Ghazzai et al., and Lee et al. do not reach the target rate, Zhang et al. and Yanmaz et al. do succeed. That Yanmaz et al. meets the rate is guaranteed by Proposition 1.

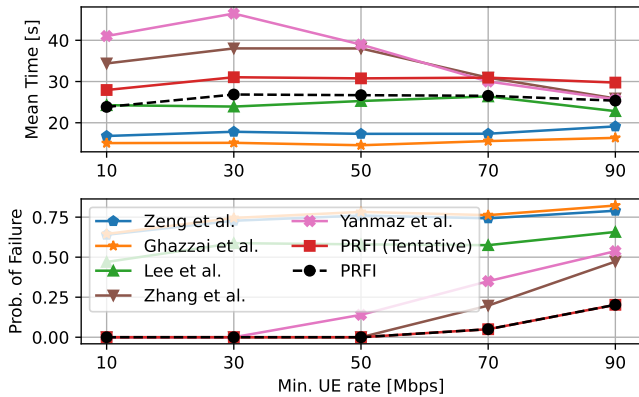


Fig. 4: \bar{T}_c and P_f vs. r_{UE}^{\min} . Some benchmarks achieve a smaller mean connection time because they only succeed in the easiest MC realizations.

PRFI (Tentative), which corresponds to the trajectory produced by Algorithm 2, is already faster than Zhang et al. and Yanmaz et al., which corroborates the efficacy of the proposed initialization. PRFI, which returns the result of applying PR to the tentative path, is significantly faster than PRFI (Tentative) and all benchmarks. This validates the adoption of PR.

The second experiment studies the influence of r_{UE}^{\min} on the expectation of the connection time, which is the cost in (9). To this end, Fig. 4 plots the mean connection time $\bar{T}_c \triangleq \mathbb{E}[T_c(\mathbf{Q}(\cdot)) \mid T_c(\mathbf{Q}(\cdot)) < \infty]$ and the probability of failure $P_f \triangleq \mathbb{P}[T_c(\mathbf{Q}(\cdot)) = \infty]$ vs. r_{UE}^{\min} . In other words, \bar{T}_c is the average of the connection time in the successful MC realizations ($\exists t : r_{UE}(\mathbf{Q}(t)) \geq r_{UE}^{\min}$) whereas P_f quantifies the fraction of unsuccessful MC realizations.

Observe that Zeng et al., Ghazzai et al., and Lee et al. have a lower \bar{T}_c than PRFI. However, looking at their P_f reveals that this is because they only succeed in a small fraction of the MC realizations. Zhang et al. and Yanmaz et al. are outperformed by PRFI in both metrics. Note again that PRFI is considerably faster than PRFI (Tentative), which again corroborates the efficacy of the proposed approach.

The next experiment studies the influence of the distance $d_{BS}^{UE} = \|\mathbf{q}_{BS} - \mathbf{q}_{UE}\|$ on \bar{T}_c and P_f . To this end, Fig. 5 plots \bar{T}_c and P_f vs. d_{BS}^{UE} . In this figure, for a given value d on the x-axis, $\check{d}_{BS}^{UE} = d - 20$ m and $\hat{d}_{BS}^{UE} = d + 20$ m. As expected, both \bar{T}_c and P_f increase with d_{BS}^{UE} . PRFI is seen to yield the best performance by far even for large values of d_{BS}^{UE} .

The next experiment quantifies how often the PRFI path is guaranteed to be optimal. The metric adopted to this end is the *probability of guaranteed optimality*, which is the fraction of MC realizations in which the optimality conditions in Sec. V-C hold. Most of the times, this probability is nearly 1. To reduce this metric to more interesting values, the problem is made more challenging by placing the BS and UE at opposite corners and disabling a randomly selected set of flight grid points. Fig. 6 plots the probability of guaranteed optimality and infeasibility vs. r_{CC} for different fractions of disabled grid points. The probability of infeasibility reflects the fraction of MC realizations in which no feasible trajectory exists. It is

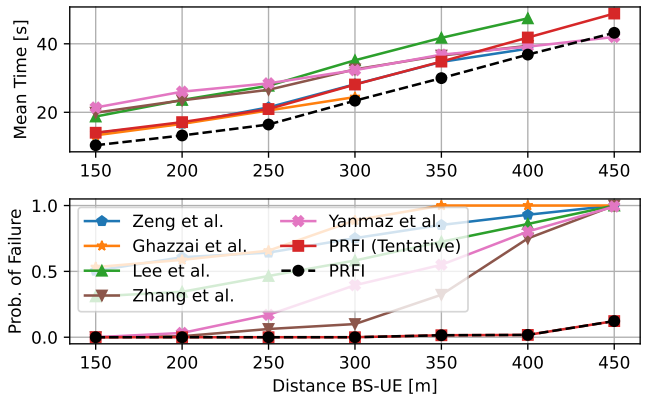


Fig. 5: \bar{T}_c and P_f vs. mean $\|\mathbf{q}_{UE} - \mathbf{q}_{BS}\|$ ($r_{UE}^{\min} = 90$ Mbps).

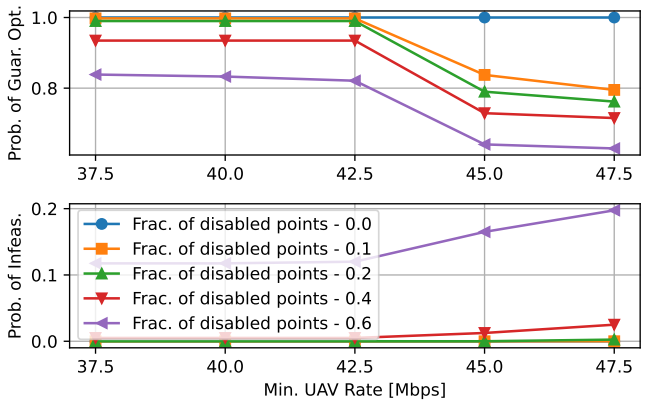


Fig. 6: Probability of guaranteed optimality and infeasibility vs. r_{CC} (The height of each building is uniformly distributed between 20 m and 40 m, $N_z^{\text{grid}} = 4$, $r_{UE}^{\min} = 10$ Mbps).

observed that PRFI yields an optimal path unless the fraction of disabled points and r_{CC} are *simultaneously* sufficiently large. It is also seen that, when an optimal path is not returned, it is because no feasible path even exists.

C. Moving UE

This section studies the performance of PRFI for moving UEs; cf. Sec. VI. Due to space restrictions, the focus will be on maximizing the transferred data. The UE follows a random trajectory of 300 seconds at a speed of 2 m/s whose initial position is generated as the UE location in Sec. VIII-B. Throughout, the height of each building at each MC realization is uniformly distributed between 20 m and 75 m.

An example of such a trajectory is shown in Fig. 7.

For the setup at hand, the benchmarks in the previous section are adapted so that the UAVs fly on $\bar{\mathcal{F}}_G$, since this simplifies the computation of the transferred data. At every time step, each UAV either stays at its current grid point or flies to an adjacent one. In all algorithms, the UAVs take off vertically at the BS until $\mathbf{p}_{BS}^{\text{top}}$. The rest of the trajectory is as follows:

- Zeng et al. [29]: at time step n , the UAV flies towards the adjacent grid point that is closest to $\mathbf{p}_{\text{mid}}[n + 1] \triangleq$

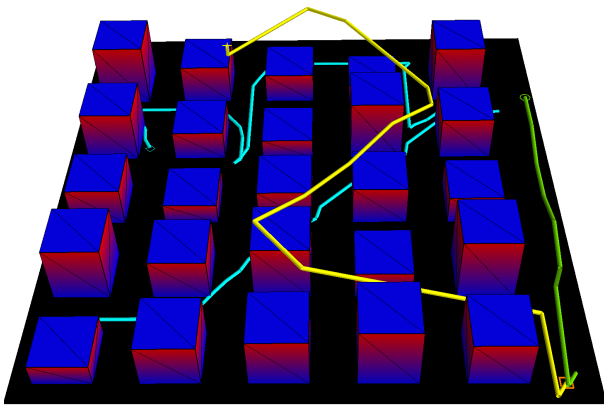


Fig. 7: An example of the UAV trajectories provided by Algorithm 6.

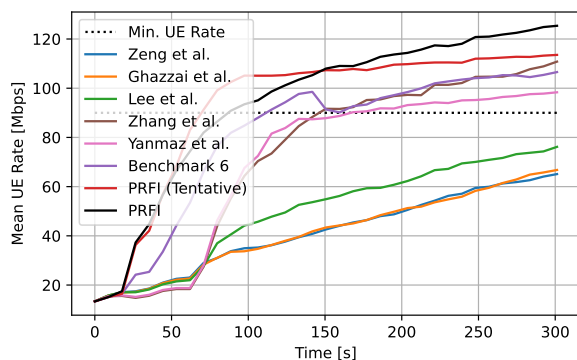


Fig. 8: Mean UE rate vs. t ($r_{\text{UE}}^{\min} = 90$ Mbps).

$(\mathbf{p}_{\text{BS}}^{\text{top}} + \mathbf{p}_{\text{UE}}^{\text{top}}[n+1])/2$, where $\mathbf{p}_{\text{UE}}^{\text{top}}[n+1] \triangleq [x_{\text{UE}}[n+1], y_{\text{UE}}[n+1], h_{\text{top}}]^T$.

- Ghazzai et al. [8]: at each time step, the UAV flies to the adjacent grid point that maximizes the UE rate predicted by the channel model in [1].
- Lee et al. [13]: at time step n , UAV-1 flies to the adjacent grid point that is closest to $\mathbf{p}_{\text{mid}}[n+1]$ and UAV-2 flies to the adjacent grid point that is closest to $\mathbf{p}_{\text{UE}}^{\text{top}}[n+1]$.
- Zhang et al. [31]: UAV-1 remains at $\mathbf{p}_{\text{BS}}^{\text{top}}$ and, at each time step, UAV-2 flies to the adjacent grid point that maximizes the UE rate in the next time step.
- Yanmaz et al. [26]: at time step n , UAV-1 remains at $\mathbf{p}_{\text{BS}}^{\text{top}}$ and UAV-2 flies to the adjacent grid point that is closest to $\mathbf{p}_{\text{UE}}^{\text{top}}[n+1]$.
- Benchmark 6: cf. Appendix E. The parameters of this benchmark are $N_{\text{replan}} = 15$ and $N_{\text{known}} = 17$.

These algorithms are compared with PRFI (Tentative) and PRFI, which respectively correspond to Algorithms 5 and 6.

Fig. 8 plots the MC average of the UE rate vs. t . As expected, PRFI (Tentative) attains r_{UE}^{\min} before PRFI but the latter yields a larger rate in the long term. This is because PRFI (Tentative) aims at minimizing outage time whereas PRFI pursues the maximization of the total transferred data.

Fig. 9 plots the total transferred data vs. t . PRFI offers the greatest slope, which implies that the margin by which it outperforms its competitors increases as time progresses.

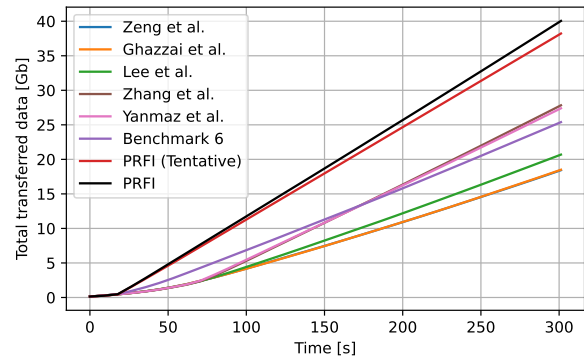


Fig. 9: Total transferred data vs. t ($\hat{d}_{\text{BS}}^{\text{UE}} = 130$ m, $\hat{d}_{\text{BS}}^{\text{UE}} = 170$ m, $r_{\text{UE}}^{\min} = 60$ Mbps).

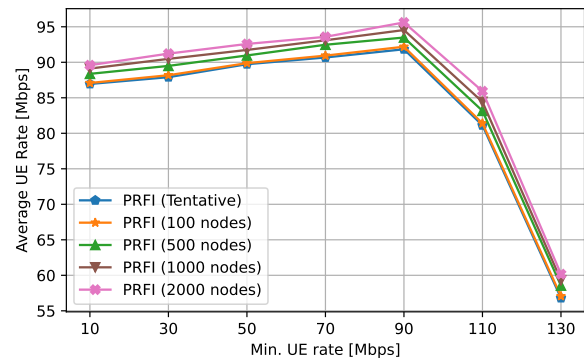


Fig. 10: Average UE rate vs. r_{UE}^{\min} (800 MC realizations).

The difference between PRFI and PRFI (Tentative) is not very large, which suggests that the proposed initialization is nearly optimal and, therefore, one may consider bypassing Algorithm 6 to reduce computational cost.

To investigate how to set the parameters of PRFI, Fig. 10 plots the average UE rate vs. r_{UE}^{\min} for different numbers C of drawn CPs in the PR step. To make differences between parameter values more conspicuous, an infinite building absorption is adopted. As expected, the greater C , the higher the average UE rate, but with diminishing returns: for example, the difference between $C = 100$ and $C = 1000$ is much more significant than between $C = 1000$ and $C = 2000$.

Although r_{UE}^{\min} does not affect the optimal path, it determines which suboptimal path PRFI returns. To select it the best way, observe from Fig. 10 that the average UE rate increases slowly when r_{UE}^{\min} is below a certain value and decreases quickly afterwards. This suggests that it is preferable to select a reasonably small r_{UE}^{\min} in practice.

Fig. 11 aims at analyzing the influence of the initial $d_{\text{BS}}^{\text{UE}}$ on the mean UE rate and fraction of outage time. The latter is defined as the fraction of time where $r_{\text{UE}}(\mathbf{Q}(t), \mathbf{q}_{\text{UE}}(t)) < r_{\text{UE}}^{\min}$. For a given value d on the x-axis, $\hat{d}_{\text{BS}}^{\text{UE}} = d - 20$ m and $\hat{d}_{\text{BS}}^{\text{UE}} = d + 20$ m. As expected, PRFI provides the highest average UE rate and lowest fraction of outage time. Note, however, that PRFI (Tentative) attains a lower fraction of outage time than PRFI. This is because the former precisely targets this objective; cf. Sec. VI-A.

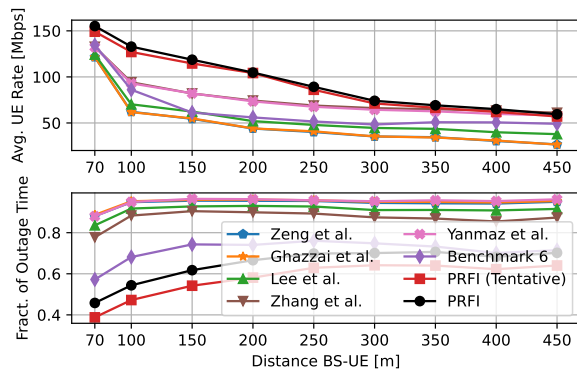


Fig. 11: Influence of the initial d_{BS}^{UE} on performance (800 realizations, $r_{UE}^{\min} = 110$ Mbps).

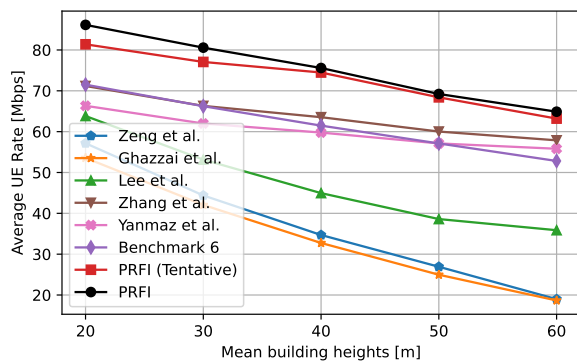


Fig. 12: Average UE rate vs. mean building height ($r_{UE}^{\min} = 100$ Mbps).

The final experiment studies the influence of the environment. To this end, Fig. 12 depicts the average UE rate vs. the mean building height. For each h on the horizontal axis, the height of each building at each MC realization is uniformly distributed between $h - 20$ m and $h + 20$ m. As expected, a greater mean height of the buildings results in a performance degradation. This is because a greater building size constrains the possible trajectories and impairs the propagation conditions by decreasing channel gain, which limits the locations where the UAVs can provide r_{UE}^{\min} to the UE and the CPs where the UAVs receive r_{CC} . Despite this fact, the proposed algorithm widely outperforms the benchmarks.

IX. CONCLUSIONS

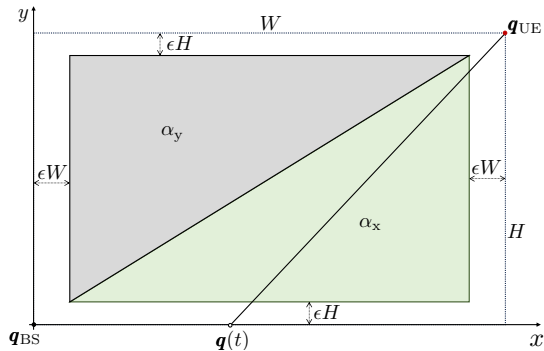
This paper developed a framework for path planning of multiple aerial relays that approximately optimizes communication metrics while accommodating arbitrary constraints on the flight region. The idea is to build upon the celebrated PR algorithm, which finds a shortest path through a random graph of CPs. To cope with the need for a large number of CPs in plain PR, a modification was proposed in which the CPs are drawn around a tentative path. This approach was applied to serve both static and moving users with any number of UAVs. To this end, heuristic rules leading to tentative paths with theoretical guarantees were proposed. Numerical results demonstrate the merits of the proposed algorithms. Future

work will investigate alternative sampling strategies for PR and approaches for data collection from terrestrial wireless sensors using UAVs.

REFERENCES

- [1] A. Al-Hourani, S. Kandeepan, and S. Lardner. Optimal LAP altitude for maximum coverage. *IEEE Wireless Commun. Lett.*, 3(6):569–572, 2014.
- [2] O. V. P. Arista, O. R. V. Barona, and R. S. Nuñez-Cruz. Development of an efficient path planning algorithm for indoor navigation. In *Int. Conf. Electr. Eng., Comput. Sci. Automat. Control*, pages 1–6, 2021.
- [3] H. Asano, H. Okada, C. B. Naila, and M. Katayama. Flight model using Voronoi tessellation for a delay-tolerant wireless relay network using drones. *IEEE Access*, 9:13064–13075, 2021.
- [4] J. Chen and D. Gesbert. Optimal positioning of flying relays for wireless networks: A LOS map approach. In *Proc. IEEE Int. Conf. Commun.*, pages 1–6, Paris, France, May 2017.
- [5] J. Chen, U. Mitra, and D. Gesbert. 3D urban UAV relay placement: Linear complexity algorithm and analysis. *IEEE Trans. Wireless Commun.*, 20(8):5243–5257, Mar. 2021.
- [6] Q. Chen. Joint trajectory and resource optimization for UAV-enabled relaying systems. *IEEE Access*, 8:24108–24119, Jan. 2020.
- [7] france24.com. No power, no phone, no transport – Spain in a panic. Technical report, 2025.
- [8] H. Ghazzai, M. Ben-Ghorbel, A. Kessler, and M. J. Hossain. Trajectory optimization for cooperative dual-band UAV swarms. In *Proc. IEEE Global Commun. Conf.*, pages 1–7, 2018.
- [9] S. Hong, S. U. Lee, X. Huang, M. Khonji, R. Alyassi, and B. C. Williams. An anytime algorithm for chance constrained stochastic shortest path problems and its application to aircraft routing. In *Proc. IEEE Int. Conf. Robot. Autom.*, pages 475–481, Oct. 2021.
- [10] X. Jiang, Z. Wu, Z. Yin, W. Yang, and Z. Yang. Trajectory and communication design for UAV-relayed wireless networks. *IEEE Wireless Commun. Lett.*, 8(6):1600–1603, Jul. 2019.
- [11] L. E. Kavraki, P. Svestka, J. C. Latombe, and M. H. Overmars. Probabilistic roadmaps for path planning in high-dimensional configuration spaces. *IEEE Trans. Robot. Autom.*, 12(4):566–580, 1996.
- [12] A. A. Khuwaja, Y. Chen, and G. Zheng. Effect of user mobility and channel fading on the outage performance of UAV communications. *IEEE Wireless Commun. Lett.*, 9(3):367–370, Nov. 2020.
- [13] J. Lee and V. Friderikos. Trajectory planning for multiple UAVs in UAV-aided wireless relay network. In *Proc. IEEE Int. Conf. Commun.*, pages 1–6, 2022.
- [14] T. Liu, M. Cui, G. Zhang, Q. Wu, X. Chu, and J. Zhang. 3D trajectory and transmit power optimization for UAV-enabled multi-link relaying systems. *IEEE Trans. Green Commun. Netw.*, 5(1):392–405, Dec. 2021.
- [15] K. Mehlhorn and P. Sanders. *Algorithms and Data Structures: The Basic Toolbox*. Springer Publishing Company, 1 edition, 2008.
- [16] N. Patwari and P. Agrawal. NeSh: a joint shadowing model for links in a multi-hop network. In *Proc. IEEE Int. Conf. Acoust., Speech, Signal Process.*, pages 2873–2876, Las Vegas, NV, Mar. 2008.
- [17] D. Romero and S.-J. Kim. Radio map estimation: A data-driven approach to spectrum cartography. *IEEE Signal Process. Mag.*, 39(6):53–72, 2022.
- [18] D. Romero, D. Lee, and G. B. Giannakis. Blind radio tomography. *IEEE Trans. Signal Process.*, 66(8):2055–2069, Jan. 2018.
- [19] D. Romero, P. Q. Viet, and R. Shrestha. Aerial base station placement via propagation radio maps. *IEEE Trans. Commun.*, 72(9):5349–5364, Sep. 2024.
- [20] Z. Sun, D. Yang, L. Xiao, L. Cuthbert, F. Wu, and Y. Zhu. Joint energy and trajectory optimization for UAV-enabled relaying network with multi-pair users. *IEEE Trans. Cogn. Commun. Netw.*, 7(3):939–954, Dec. 2021.
- [21] P. Q. Viet and D. Romero. Aerial base station placement: A tutorial introduction. *IEEE Commun. Mag.*, 60(5):44–49, 2022.
- [22] P. Q. Viet and D. Romero. Probabilistic roadmaps for aerial relay path planning. In *IEEE Glob. Commun. Conf.*, 2023.
- [23] Pham Q. Viet and Daniel Romero. Path planning for aerial relays via probabilistic roadmaps, Jan. 2026.
- [24] H. Wang, G. Ren, J. Chen, G. Ding, and Y. Yang. Unmanned aerial vehicle-aided communications: Joint transmit power and trajectory optimization. *IEEE Wireless Commun. Lett.*, 7(4):522–525, 2018.
- [25] H. Yang, J. Zhang, S. H. Song, and K. B. Lataief. Connectivity-aware UAV path planning with aerial coverage maps. In *Proc. IEEE Wireless Commun. Netw. Conf.*, pages 1–6, 2019.

Fig. 13: Scenario for the analysis of the influence of the objective function on the optimal trajectory.



- [26] E. Yanmaz. Positioning aerial relays to maintain connectivity during drone team missions. *Ad Hoc Networks*, 128:102800, 2022.
- [27] E. Yanmaz. Joint or decoupled optimization: Multi-UAV path planning for search and rescue. *Ad Hoc Networks*, 138:103018, Jan. 2023.
- [28] E. Yanmaz, H. M. Balanji, and İ. Güven. Dynamic multi-UAV path planning for multi-target search and connectivity. *IEEE Transactions on Vehicular Technology*, 73(7):10516–10528, Feb. 2024.
- [29] Y. Zeng, R. Zhang, and T. J. Lim. Throughput maximization for UAV-enabled mobile relaying systems. *IEEE Trans. Commun.*, 64(12):4983–4996, Dec. 2016.
- [30] G. Zhang, X. Ou, M. Cui, Q. Wu, S. Ma, and W. Chen. Cooperative UAV enabled relaying systems: Joint trajectory and transmit power optimization. *IEEE Trans. Green Commun. Netw.*, 6(1):543–557, 2022.
- [31] G. Zhang, H. Yan, Y. Zeng, M. Cui, and Y. Liu. Trajectory optimization and power allocation for multi-hop UAV relaying communications. *IEEE Access*, 6:48566–48576, 2018.
- [32] S. Zhang, H. Zhang, Q. He, K. Bian, and L. Song. Joint trajectory and power optimization for uav relay networks. *IEEE Commun. Lett.*, 22(1):161–164, Oct. 2018.
- [33] N. Zhao, W. Lu, M. Sheng, Y. Chen, J. Tang, F. R. Yu, and K. Wong. UAV-assisted emergency networks in disasters. *IEEE Wireless Commun.*, 26(1):45–51, Feb. 2019.

APPENDIX A

INFLUENCE OF THE OBJECTIVE ON THE TRAJECTORY

This appendix analyzes how the selection of the objective function determines the optimal trajectory.

The UE is assumed static; the case of a moving UE is left for future work. Consider a simple scenario where a single UAV is used. The BS and the UE are at opposite corners of a building; see Fig. 13. Specifically, the BS and the UE are respectively at the ground locations $\mathbf{q}_{\text{BS}} = [0, 0]^\top$ and $\mathbf{q}_{\text{UE}} = [W, H]^\top$, where H and W are two constants satisfying $H < W$. The floor plan of the building spans the rectangle $[\epsilon W, W - \epsilon W] \times [\epsilon H, H - \epsilon H]$, where $\epsilon > 0$ is arbitrarily small. The UAV flies with speed v_{max} from the initial location \mathbf{q}_{BS} . For simplicity, the height of the UAV is 0. Thus, its position at time instant t can be represented by the 2D vector $\mathbf{q}(t) \in \mathbb{R}^2$.

The UAV transmits with fixed power P_t , wavelength λ , and bandwidth B . For simplicity, the BS and UAV transmit on orthogonal channel resources and, thus, they do not interfere each other. The transmit power and bandwidth of the BS are sufficiently large so that the UE rate coincides with the rate of the UAV-UE link; cf. Sec. III-A. The tomographic model (see Sec. III-B) is adopted. The absorption of the building is $\alpha_y = +\infty$ dB/m when $Wy \geq Hx$ and $\alpha_x > 0$ when $Wy < Hx$. The noise power at the UE is σ^2 .

The paper considers three objectives: (9), (10), and (11). Since the UE does not move, (9) and (10) are equivalent. Thus, the following comparison focuses on the *connection time* (9) and the *transferred data* (11) objectives. Regarding (9), recall that the UE is said to be connected once $r_{\text{UE}}(t) \geq r_{\text{UE}}^{\text{min}}$. When it comes to (11), there is no minimum required rate.

Suppose that the time horizon is $t_1 \triangleq W/v_{\text{max}}$. In this case, it can be easily seen that the optimal trajectory according to (9) and (11) is necessarily one of the following:

- \mathcal{T}_x : In this trajectory, the UAV flies along the x axis from \mathbf{q}_{BS} to $[W, 0]^\top$, i.e., $\mathbf{q}(t) = [v_{\text{max}}t, 0]^\top$, $t \in [0, t_1]$.
- \mathcal{T}_y : In this trajectory, the UAV flies along the y axis and then stops: $\mathbf{q}(t) = [0, v_{\text{max}}t]^\top$, $\forall t \in [0, t_0]$ and $\mathbf{q}(t) = [0, H]^\top$, $\forall t \in [t_0, t_1]$, where $t_0 \triangleq H/v_{\text{max}}$. Note that the reason why the UAV stays at $\mathbf{q}(t_0) = [0, H]^\top$ instead of continuing right is to avoid losing connectivity with the BS due to the infinite absorption α_y . It does not continue to fly along the y axis either because in that case the distance to the UE would increase.

Let \mathcal{T}_{tc} and \mathcal{T}_{dat} respectively denote the optimal trajectories according to (9) and (11). If $r_{\text{UE}}^{\text{min}}$ is too large, then neither \mathcal{T}_x nor \mathcal{T}_y will result in a finite (9). Thus, suppose that $r_{\text{UE}}^{\text{min}}$ is such that the UAV can meet the requirement $r_{\text{UE}}(t) > r_{\text{UE}}^{\text{min}}$ at the end of both trajectories, i.e.,

$$r_{\text{UE}}^{\text{min}} \leq B \log_2 \left(1 + \frac{P_t \lambda^2}{16\pi^2 \sigma^2 W^2} \right). \quad (21)$$

Under this assumption, the optimal trajectory will depend on α_x . If α_x is very large, then clearly $\mathcal{T}_{\text{tc}} = \mathcal{T}_{\text{dat}} = \mathcal{T}_y$. Conversely, if α_x is very small, then clearly $\mathcal{T}_{\text{tc}} = \mathcal{T}_{\text{dat}} = \mathcal{T}_x$. The case where α_x is neither too large nor too small is addressed by the following result:

Theorem 3: Let

$$\alpha_{\text{tc}} \triangleq \frac{10}{\sqrt{(H-W)^2 + H^2}} \cdot \log_{10} \left(\frac{P_t \lambda^2 \left(2^{r_{\text{UE}}^{\text{min}}/B} - 1 \right)^{-1}}{16\pi^2 \sigma^2 ((H-W)^2 + H^2)} \right) \quad (22)$$

and let

$$\alpha_{\text{dat}} \triangleq \frac{1}{\hat{D}^{(x)}} \left(B \log_2 \left(\frac{P_t \lambda^2}{16\pi^2 \sigma^2} \right) \frac{W}{v_{\text{max}}} - B \log_2 \left(1 + \frac{P_t \lambda^2}{16\pi^2 \sigma^2 W^2} \right) \frac{W-H}{v_{\text{max}}} - \hat{D}^{(x)} \right), \quad (23)$$

where

$$\hat{D}^{(x)} \triangleq B \frac{\log_2 10}{20v_{\text{max}}} \left(W \sqrt{W^2 + H^2} + H^2 \tanh^{-1} \left(\frac{W}{\sqrt{W^2 + H^2}} \right) \right) \quad (24)$$

and

$$\hat{D}^{(x)} \triangleq B t_1 \log_2 (W^2 + H^2) - 2B t_1 \log_2 e + 2B t_0 \log_2 e \tan^{-1} \left(\frac{W}{H} \right). \quad (25)$$

If (21) holds and

$$\alpha_{\text{tic}} < \alpha_x < \alpha_{\text{dat}}, \quad (26)$$

then $\mathcal{T}_{\text{tic}} = \mathcal{T}_y$ and $\mathcal{T}_{\text{dat}} = \mathcal{T}_x$.

Proof: The proof will first derive the UE rate over time for both \mathcal{T}_x and \mathcal{T}_y . Then, it will show that (i) if $\alpha_{\text{tic}} (r_{\text{UE}}^{\min}) < \alpha_x$, then $\mathcal{T}_{\text{tic}} = \mathcal{T}_y$; and (ii), if $\alpha_x < \alpha_{\text{dat}}$, then $\mathcal{T}_{\text{dat}} = \mathcal{T}_x$.

Due to the tomographic model, the channel gain at time instant t between the UAV and the UE for sufficiently small ϵ is

$$\bar{\gamma}(\alpha, t) = 20 \log_{10} \left(\frac{\lambda}{4\pi \|\mathbf{q}(t) - \mathbf{q}_{\text{UE}}\|} \right) - \alpha \|\mathbf{q}(t) - \mathbf{q}_{\text{UE}}\|, \quad (27)$$

where α is the absorption. In the case of \mathcal{T}_x , one has $\alpha = \alpha_x$. In the case of \mathcal{T}_y , one has $\alpha = \alpha_y = +\infty$ for $t \in [0, t_0)$ and $\alpha = 0$ for $t \in [t_0, t_1]$. In natural units, (27) reads as

$$\gamma(\alpha, t) = \left(\frac{\lambda}{4\pi \|\mathbf{q}(t) - \mathbf{q}_{\text{UE}}\|} \right)^2 \frac{1}{10^{\alpha \|\mathbf{q}(t) - \mathbf{q}_{\text{UE}}\|/10}}. \quad (28)$$

The resulting UE rate is, therefore,

$$r_{\text{UE}}(\alpha, t) \quad (29a)$$

$$= B \log_2 \left(1 + \frac{P_1}{\sigma^2} \gamma(\alpha, t) \right) \quad (29b)$$

$$= B \log_2 \left(1 + \frac{P_1 \lambda^2}{16\pi^2 \sigma^2 \|\mathbf{q}(t) - \mathbf{q}_{\text{UE}}\|^2 10^{\alpha \|\mathbf{q}(t) - \mathbf{q}_{\text{UE}}\|/10}} \right). \quad (29c)$$

Let $r_{\text{UE}}^{(y)}(t)$ be the UE rate at time instant t when the UAV follows \mathcal{T}_y . For $t \in [0, t_0)$, one has that $\alpha = \alpha_y = +\infty$ and, therefore,

$$r_{\text{UE}}^{(y)}(t) \approx r_{\text{UE}}(\infty, t) = 0. \quad (30)$$

On the other hand, for $t \in [t_0, t_1]$, one has that $\alpha = 0$ and, as a result,

$$r_{\text{UE}}^{(y)}(t) = B \log_2 \left(1 + \frac{P_1 \lambda^2}{16\pi^2 \sigma^2 \|\mathbf{q}(t) - \mathbf{q}_{\text{UE}}\|^2} \right) \quad (31a)$$

$$= B \log_2 \left(1 + \frac{P_1 \lambda^2}{16\pi^2 \sigma^2 W^2} \right) \stackrel{(21)}{\geq} r_{\text{UE}}^{\min}. \quad (31b)$$

Similarly, let $r_{\text{UE}}^{(x)}(t)$ be the UE rate at time instant t when the UAV follows \mathcal{T}_x . Since in this case $\alpha = \alpha_x \forall t \in [0, t_1]$, it holds that

$$r_{\text{UE}}^{(x)}(t) \quad (32a)$$

$$= r_{\text{UE}}(\alpha_x, t) \quad (32b)$$

$$= B \log_2 \left(1 + \frac{P_1 \lambda^2}{16\pi^2 \sigma^2 \|\mathbf{q}(t) - \mathbf{q}_{\text{UE}}\|^2 10^{\alpha_x \|\mathbf{q}(t) - \mathbf{q}_{\text{UE}}\|/10}} \right). \quad (32c)$$

Next, it will be shown that $\mathcal{T}_{\text{tic}} = \mathcal{T}_y$ whenever $\alpha_{\text{tic}} < \alpha_x$. To this end, note from (22) that $\alpha_{\text{tic}} < \alpha_x$ if and only if

$$\frac{10}{\sqrt{(H-W)^2 + H^2}} \log_{10} \left(\frac{P_1 \lambda^2 (2^{r_{\text{UE}}^{\min}/B} - 1)^{-1}}{16\pi^2 \sigma^2 ((H-W)^2 + H^2)} \right) < \alpha_x. \quad (33)$$

Solving for r_{UE}^{\min} yields

$$r_{\text{UE}}^{\min} \quad (34a)$$

$$> B \log_2 \left(1 + \frac{P_1 \lambda^2}{16\pi^2 \sigma^2 ((H-W)^2 + H^2) 10^{\alpha_x \sqrt{(H-W)^2 + H^2}/10}} \right) \quad (34b)$$

$$= B \log_2 \left(1 + \frac{P_1 \lambda^2}{16\pi^2 \sigma^2 \|\mathbf{q}(t_0) - \mathbf{q}_{\text{UE}}\|^2 10^{\alpha_x \|\mathbf{q}(t_0) - \mathbf{q}_{\text{UE}}\|/10}} \right) \quad (34c)$$

$$= r_{\text{UE}}^{(x)}(t_0). \quad (34d)$$

Combining this inequality with (31b) results in

$$r_{\text{UE}}^{(x)}(t_0) < r_{\text{UE}}^{\min} \stackrel{(31b)}{\leq} r_{\text{UE}}^{(y)}(t_0) \quad (35)$$

and, therefore, $\mathcal{T}_{\text{tic}} = \mathcal{T}_y$.

Finally, it will be shown that $\mathcal{T}_{\text{dat}} = \mathcal{T}_x$ if $\alpha_x < \alpha_{\text{dat}}$. The amount of transferred data when the UAV follows \mathcal{T}_y is given by

$$D_{\text{UE}}^{(y)}(t_1) \triangleq \int_0^{t_1} r_{\text{UE}}^{(y)}(\tau) d\tau \quad (36a)$$

$$= \int_0^{t_0} r_{\text{UE}}^{(y)}(\tau) d\tau + \int_{t_0}^{t_1} r_{\text{UE}}^{(y)}(\tau) d\tau \quad (36b)$$

$$= 0 + B \log_2 \left(1 + \frac{P_1 \lambda^2}{16\pi^2 \sigma^2 W^2} \right) (t_1 - t_0) \quad (36c)$$

$$= B \log_2 \left(1 + \frac{P_1 \lambda^2}{16\pi^2 \sigma^2 W^2} \right) \frac{W - H}{v_{\max}}. \quad (36d)$$

The amount of transferred data when the UAV follows \mathcal{T}_x is given by

$$D_{\text{UE}}^{(x)}(t_1) \quad (37a)$$

$$\triangleq \int_0^{t_1} r_{\text{UE}}^{(x)}(\tau) d\tau \quad (37b)$$

$$> \int_0^{t_1} B \log_2 \left(\frac{P_1 \lambda^2}{16\pi^2 \sigma^2 \|\mathbf{q}(\tau) - \mathbf{q}_{\text{UE}}\|^2 10^{\alpha_x \|\mathbf{q}(\tau) - \mathbf{q}_{\text{UE}}\|/10}} \right) d\tau \quad (37c)$$

$$= B \log_2 \left(\frac{P_1 \lambda^2}{16\pi^2 \sigma^2} \right) t_1 - \hat{D}^{(x)}(t_1) - \alpha_x \check{D}^{(x)}(t_1) \quad (37d)$$

$$\triangleq \check{D}_{\text{UE}}^{(x)}(t_1), \quad (37e)$$

where

$$\hat{D}^{(x)}(t_1) \triangleq B \int_0^{t_1} \log_2 \left(\|\mathbf{q}(\tau) - \mathbf{q}_{\text{UE}}\|^2 \right) d\tau \quad (38a)$$

$$\check{D}^{(x)}(t_1) \triangleq B \frac{\log_2 10}{10} \int_0^{t_1} \|\mathbf{q}(\tau) - \mathbf{q}_{\text{UE}}\| d\tau. \quad (38b)$$

Since $\mathbf{q}(t) = [v_{\max}t, 0]^\top$, it can be seen that

$$\hat{D}^{(x)}(t_1) \quad (39a)$$

$$= \frac{B \log_2 e}{v_{\max}} \left((v_{\max}t_1 - W) \log \left((v_{\max}t_1 - W)^2 + H^2 \right) \right. \quad (39b)$$

$$\left. + 2H \tan^{-1} \left(\frac{v_{\max}t_1 - W}{H} \right) - 2v_{\max}t_1 \right)$$

$$- \frac{B \log_2 e}{v_{\max}} \left((-W) \log \left((-W)^2 + H^2 \right) \right. \quad (39c)$$

$$\left. + 2H \tan^{-1} \left(\frac{-W}{H} \right) \right)$$

$$= Bt_1 \log_2 (W^2 + H^2) - 2Bt_1 \log_2 e \quad (39c)$$

$$+ 2Bt_0 \log_2 e \tan^{-1} \left(\frac{W}{H} \right)$$

$$= \hat{D}^{(x)} \quad (39d)$$

and

$$\tilde{D}^{(x)}(t_1) \quad (40a)$$

$$= B \frac{\log_2 10}{20v_{\max}} \left((v_{\max}t_1 - W) \sqrt{(v_{\max}t_1 - W)^2 + H^2} \right. \quad (40b)$$

$$\left. - H^2 \tanh^{-1} \left(\frac{W - v_{\max}t_1}{\sqrt{(v_{\max}t_1 - W)^2 + H^2}} \right) \right)$$

$$- B \frac{\log_2 10}{20v_{\max}} \left((-W) \sqrt{(-W)^2 + H^2} \right. \quad (40c)$$

$$\left. - H^2 \tanh^{-1} \left(\frac{W}{\sqrt{W^2 + H^2}} \right) \right)$$

$$= B \frac{\log_2 10}{20v_{\max}} \left(W \sqrt{W^2 + H^2} + H^2 \tanh^{-1} \left(\frac{W}{\sqrt{W^2 + H^2}} \right) \right) \quad (40c)$$

$$= \tilde{D}^{(x)}. \quad (40d)$$

From (37), $\tilde{D}_{\text{UE}}^{(x)}(t_1)$ is a lower bound of $D_{\text{UE}}^{(x)}(t_1)$. It can also be seen that $\tilde{D}_{\text{UE}}^{(x)}(t_1)$ is an upper bound for $D_{\text{UE}}^{(y)}(t_1)$. To this end, note from (23) that

$$\alpha_x < \alpha_{\text{dat}} = \frac{1}{\tilde{D}^{(x)}} \left(B \log_2 \left(\frac{P_t \lambda^2}{16\pi^2 \sigma^2} \right) \frac{W}{v_{\max}} \right. \quad (41)$$

$$\left. - B \log_2 \left(1 + \frac{P_t \lambda^2}{16\pi^2 \sigma^2 W^2} \right) \frac{W - H}{v_{\max}} - \hat{D}^{(x)} \right).$$

Rearranging terms, one finds that

$$D_{\text{UE}}^{(y)}(t_1) = B \log_2 \left(1 + \frac{P_t \lambda^2}{16\pi^2 \sigma^2 W^2} \right) \frac{W - H}{v_{\max}} \quad (42a)$$

$$< B \log_2 \left(\frac{P_t \lambda^2}{16\pi^2 \sigma^2} \right) \frac{W}{v_{\max}} - \hat{D}^{(x)} - \alpha_x \tilde{D}^{(x)} \quad (42b)$$

$$= \tilde{D}_{\text{UE}}^{(x)}(t_1) \quad (42c)$$

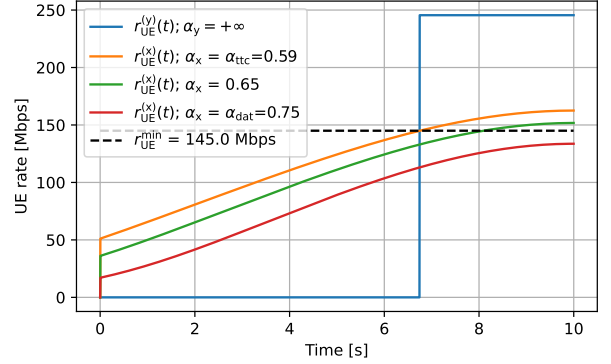
Thus, to sum up,

$$D_{\text{UE}}^{(y)}(t_1) < \tilde{D}_{\text{UE}}^{(x)}(t_1) < D_{\text{UE}}^{(x)}(t_1) \quad (43)$$

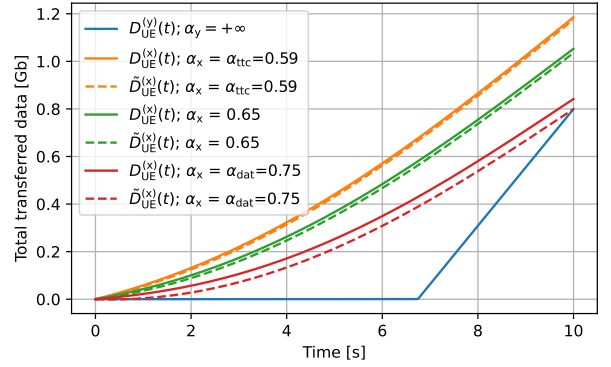
and, as a result, $\mathcal{T}_{\text{dat}} = \mathcal{T}_x$. ■

TABLE III

Notation	Physical meaning	Simulation value
$W \times H$	Building dimensions	40×27 m
ϵ	Distance from the building edge	10^{-3} m
v_{\max}	Maximum UAV speed	4 m/s
P_t	UAV transmit power	0.1 W
f	Carrier frequency	6 GHz
B	Bandwidth	20 MHz
σ^2	Noise power	-97 dBm
r_{UE}^{\min}	Minimum required UE rate	145 Mbps



(a)



(b)

Fig. 14: UE rate and the amount of transferred data over time; $r_{\text{UE}}^{\min} = 145$ Mbps.

In words, when α_x takes intermediate values, the optimal UAV trajectory depends on whether one adopts (9) or (11).

A numerical example will be presented to illustrate Theorem 3. The simulation parameters are listed on Table III. They were chosen so that (21) holds. As a result, one has $\alpha_{\text{ttc}} = 0.59$ and $\alpha_{\text{dat}} = 0.75$.

Fig. 14 shows the UE rate and the amount of transferred data over time when the UAV follows \mathcal{T}_x and \mathcal{T}_y . It is observed that:

- If $\alpha_x > \alpha_{\text{ttc}}$, then \mathcal{T}_y minimizes the connection time ($\mathcal{T}_{\text{ttc}} = \mathcal{T}_y$); cf. Fig. 14a.
- If $\alpha_x < \alpha_{\text{dat}}$, then \mathcal{T}_x maximizes the amount of transferred data ($\mathcal{T}_{\text{dat}} = \mathcal{T}_x$); cf. Fig. 14b.
- When $\alpha_{\text{ttc}} < \alpha_x < \alpha_{\text{dat}}$, one has that $\mathcal{T}_{\text{ttc}} = \mathcal{T}_y$ and $\mathcal{T}_{\text{dat}} = \mathcal{T}_x$. This is precisely as predicted by Theorem 3.

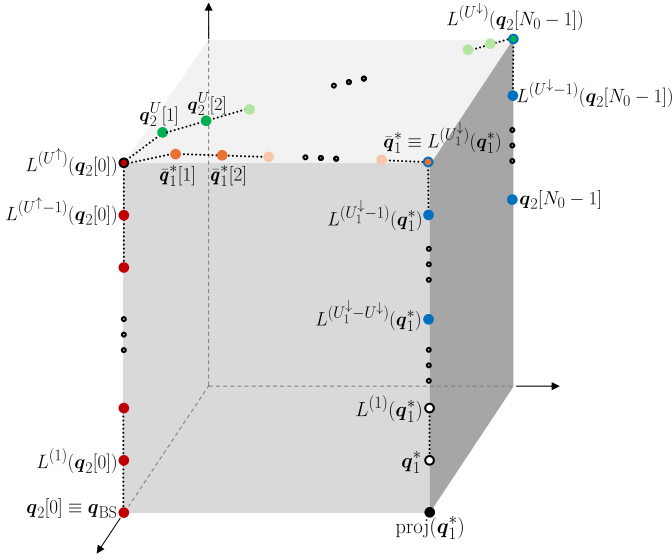


Fig. 15: Illustration of the trajectory constructed in the proof of Theorem 1.

APPENDIX B PROOF OF THEOREM 1

Let $p_2 \triangleq \{q_2[0], q_2[1], \dots, q_2[N_0 - 1]\}$ be the path for UAV-2 returned by Algorithm 1. Observe that, for a given h_{\max} , there is a maximum number of times that p_2 can be lifted before the lifting operator returns the same path as its input, that is, $L^{(u)}(p_2) = L^{(u+1)}(p_2)$ for a sufficiently large u . Let U denote the smallest of such values of u , i.e., $U \triangleq \min\{u \in \mathbb{N} : L^{(u)}(p_2) = L^{(u+1)}(p_2)\}$.

If Algorithm 2 fails to provide a valid path, it necessarily fails to find a valid path at all iterations and, in particular, at the U -th iteration. Therefore, to prove the theorem, it suffices to show that the algorithm succeeds if it reaches the U -th iteration, which is the worst case. Equivalently, it has to be shown that Algorithm 2 can find a path to $\mathbb{N} \times \mathcal{D}_1$ through the extended graph corresponding to $L^{(U)}(p_2)$. Since Algorithm 2 is based on a shortest path algorithm, it will return a path to $\mathbb{N} \times \mathcal{D}_1$ if at least one such a path exists. Therefore, to prove the theorem, it suffices to find *any* path to $\mathbb{N} \times \mathcal{D}_1$.

To establish the existence of such a path in the extended graph, the rest of the proof will design a path for UAV-1 and show that the resulting combined path $P \triangleq \{\hat{Q}[0], \dots, \hat{Q}[N-1]\}$ is valid. With $\hat{Q}[n] = [\hat{q}_1[n], \hat{q}_2[n]]$, this means that $\hat{q}_1[N-1] \in \mathcal{D}_1$ and the following conditions hold:

C1: The rate between the BS and UAV-1 is at least $2r_{CC}$, i.e., $c(q_{BS}, \hat{q}_1[n]) \geq 2r_{CC}$ for all n , and

C2: The rate from UAV-1 to UAV-2 is at least r_{CC} , i.e., $c(\hat{q}_1[n], \hat{q}_2[n]) \geq r_{CC}$ for all n .

To simplify the exposition, the path $L^{(U)}(p_2)$ will be separated into the following subpaths:

$$p^\uparrow \triangleq \{q_2[0], L^{(1)}(q_2[0]), \dots, L^{(U^\uparrow)}(q_2[0])\}, \quad (44a)$$

$$\begin{aligned} \vec{p} \triangleq \{L^{(U^\uparrow)}(q_2[0]), q_2^{(U)}[1], \dots, q_2^{(U)}[N_U - 2], \\ L^{(U^\downarrow)}(q_2[N_0 - 1])\}, \end{aligned} \quad (44b)$$

$$p^\downarrow \triangleq \{L^{(U^\downarrow)}(q_2[N_0 - 1]), \dots, q_2[N_0 - 1]\}, \quad (44c)$$

where

$$U^\uparrow \triangleq \min\{u \in \mathbb{N} : L^{(u)}(q_2[0]) = L^{(u+1)}(q_2[0])\} \quad (45a)$$

$$U^\downarrow \triangleq \min\{u \in \mathbb{N} : L^{(u)}(q_2[N_0 - 1]) = L^{(u+1)}(q_2[N_0 - 1])\}, \quad (45b)$$

and \vec{p} is the shortest path from $L^{(U^\uparrow)}(q_2[0])$ to $L^{(U^\downarrow)}(q_2[N_0 - 1])$ in the graph of Sec. V-A1. For each subpath in (44), a subpath will be designed for UAV-1. The resulting combined path will be valid because the last subpath ends at \mathcal{D}_1 by construction and each combined subpath will be shown to satisfy C1 and C2.

Take-off subpath (p^\uparrow): In the considered combined path, when UAV-2 follows p^\uparrow , UAV-1 follows p^\uparrow as well. Recall that the minimum separation between the UAVs was disregarded in (8) for simplicity. Thus, the combined path of UAV-1 and UAV-2 is given by

$$\begin{aligned} P^\uparrow \triangleq \left\{ \left[q_2[0], q_2[0] \right], \left[L^{(1)}(q_2[0]), L^{(1)}(q_2[0]) \right], \dots, \right. \\ \left. \left[L^{(U^\uparrow)}(q_2[0]), L^{(U^\uparrow)}(q_2[0]) \right] \right\}. \end{aligned} \quad (46)$$

C1: By hypothesis,

$$h_{\max} \leq \sqrt{[\bar{c}^{-1}(2r_{CC})]^2 - [\bar{c}^{-1}(2r_{CC} + r_{UE}^{\min})]^2}, \quad (47)$$

which implies that $h_{\max}^2 \leq [\bar{c}^{-1}(2r_{CC})]^2$ or, equivalently, $h_{\max} \leq \bar{c}^{-1}(2r_{CC})$. Thus, since $q_2[0] = q_{BS}$, $\forall \hat{q}_1 \in p^\uparrow$, it follows that $\|q_{BS} - \hat{q}_1\| \leq \|q_{BS} - L^{(U^\uparrow)}(q_2[0])\| \leq h_{\max} \leq \bar{c}^{-1}(2r_{CC})$. Noting that c is a decreasing function of the distance, yields

$$c(q_{BS}, \hat{q}_1) \geq c(q_{BS}, L^{(U^\uparrow)}(q_2[0])) \geq 2r_{CC}, \quad (48)$$

which establishes C1.

C2: trivial.

Top subpath (\vec{p}): The combined path will be divided into two parts:

Part 1: UAV-1 stays at $L^{(U^\uparrow)}(q_2[0])$ while UAV-2 follows \vec{p} in (44b). Note that, as per \vec{p} , UAV-2 flies at constant height h_{\max} from $L^{(U^\uparrow)}(q_2[0])$ to $L^{(U^\downarrow)}(q_2[N_0 - 1])$. The combined path is then

$$\begin{aligned} \vec{P}_1 \triangleq \left\{ \left[L^{(U^\uparrow)}(q_2[0]), L^{(U^\uparrow)}(q_2[0]) \right], \right. \\ \left[L^{(U^\uparrow)}(q_2[0]), q_2^{(U)}[1] \right], \dots, \left[L^{(U^\uparrow)}(q_2[0]), q_2^{(U)}[N_U - 2] \right], \\ \left. \left[L^{(U^\uparrow)}(q_2[0]), L^{(U^\downarrow)}(q_2[N_0 - 1]) \right] \right\}. \end{aligned} \quad (49)$$

C1: It follows from (48).

C2: To prove that $c(L^{(U^\uparrow)}(q_2[0]), \hat{q}_2) \geq r_{CC}$, $\forall \hat{q}_2 \in \vec{p}$, it can be observed that \vec{p} is the shortest path from $L^{(U^\uparrow)}(q_2[0])$ to $L^{(U^\downarrow)}(q_2[N_0 - 1])$, hence $\forall \hat{q}_2 \in \vec{p}$,

$$\|L^{(U^\uparrow)}(q_2[0]) - \hat{q}_2\| \leq \|L^{(U^\uparrow)}(q_2[0]) - L^{(U^\downarrow)}(q_2[N_0 - 1])\|. \quad (50)$$

Hence, it suffices to prove that $\|L^{(U^\uparrow)}(q_2[0]) - L^{(U^\downarrow)}(q_2[N_0 - 1])\| \leq \bar{c}^{-1}(r_{CC})$. To this end, recall that $q_2[N_0 -$

$1] \in \mathcal{D}_2$. Thus, when UAV-2 is at $\mathbf{q}_2[N_0 - 1]$, there exists a location $\mathbf{q}_1^* = [q_{1x}^*, q_{1y}^*, q_{1z}^*]^\top$ for UAV-1 such that

$$\mathbf{q}_1^* \in \mathcal{R}(\mathbf{q}_{BS}, 2r_{CC} + r_{UE}^{\min}) \cap \mathcal{R}(\mathbf{q}_2[N_0 - 1], r_{CC} + r_{UE}^{\min}). \quad (51)$$

It follows that $c(\mathbf{q}_{BS}, \mathbf{q}_1^*) \geq 2r_{CC} + r_{UE}^{\min}$ and $c(\mathbf{q}_2[N_0 - 1], \mathbf{q}_1^*) \geq r_{CC} + r_{UE}^{\min}$, or, equivalently, that

$$\|\mathbf{q}_{BS} - \mathbf{q}_1^*\| \leq \bar{c}^{-1}(2r_{CC} + r_{UE}^{\min}), \text{ and} \quad (52a)$$

$$\|\mathbf{q}_2[N_0 - 1] - \mathbf{q}_1^*\| \leq \bar{c}^{-1}(r_{CC} + r_{UE}^{\min}). \quad (52b)$$

Let $\bar{\mathbf{q}}_1^* = [q_{1x}^*, q_{1y}^*, h_{\max}]^\top$ and consider three points at the same height h_{\max} : $L^{(U^\uparrow)}(\mathbf{q}_2[0])$, $L^{(U^\downarrow)}(\mathbf{q}_2[N_0 - 1])$, and $\bar{\mathbf{q}}_1^*$. From the triangle inequality, one has

$$\begin{aligned} & \|L^{(U^\uparrow)}(\mathbf{q}_2[0]) - L^{(U^\downarrow)}(\mathbf{q}_2[N_0 - 1])\| \\ & \leq \|L^{(U^\uparrow)}(\mathbf{q}_2[0]) - \bar{\mathbf{q}}_1^*\| + \|L^{(U^\downarrow)}(\mathbf{q}_2[N_0 - 1]) - \bar{\mathbf{q}}_1^*\|. \end{aligned} \quad (53)$$

Since $L^{(U^\uparrow)}(\mathbf{q}_2[0]) = L^{(U^\uparrow)}(\mathbf{q}_{BS})$ and $\bar{\mathbf{q}}_1^*$ are at the same height, it follows that

$$\|L^{(U^\uparrow)}(\mathbf{q}_2[0]) - \bar{\mathbf{q}}_1^*\| \leq \|\mathbf{q}_{BS} - \mathbf{q}_1^*\| \stackrel{(52a)}{\leq} \bar{c}^{-1}(2r_{CC} + r_{UE}^{\min}). \quad (54)$$

Similarly, since $L^{(U^\downarrow)}(\mathbf{q}_2[N_0 - 1])$ and $\bar{\mathbf{q}}_1^*$ are at the same height,

$$\|L^{(U^\downarrow)}(\mathbf{q}_2[N_0 - 1]) - \bar{\mathbf{q}}_1^*\| \leq \|\mathbf{q}_2[N_0 - 1] - \mathbf{q}_1^*\| \quad (55a)$$

$$\stackrel{(52b)}{\leq} \bar{c}^{-1}(r_{CC} + r_{UE}^{\min}). \quad (55b)$$

From (54) and (55b),

$$\begin{aligned} & \|L^{(U^\uparrow)}(\mathbf{q}_2[0]) - \bar{\mathbf{q}}_1^*\| + \|L^{(U^\downarrow)}(\mathbf{q}_2[N_0 - 1]) - \bar{\mathbf{q}}_1^*\| \\ & \leq \bar{c}^{-1}(2r_{CC} + r_{UE}^{\min}) + \bar{c}^{-1}(r_{CC} + r_{UE}^{\min}). \end{aligned} \quad (56)$$

The following result provides an upper bound for the right-hand side:

Lemma 1: If Eq. (14) holds, then

$$\bar{c}^{-1}(2r_{CC} + r_{UE}^{\min}) + \bar{c}^{-1}(r_{CC} + r_{UE}^{\min}) < \bar{c}^{-1}(r_{CC}). \quad (57)$$

Proof: See Appendix C. \blacksquare

From (50), (53), (56) and Lemma 1, it holds that, $\forall \hat{\mathbf{q}}_2 \in \vec{P}$,

$$\begin{aligned} & \|L^{(U^\uparrow)}(\mathbf{q}_2[0]) - \hat{\mathbf{q}}_2\| \stackrel{(50)}{\leq} \|L^{(U^\uparrow)}(\mathbf{q}_2[0]) - L^{(U^\downarrow)}(\mathbf{q}_2[N_0 - 1])\| \\ & \stackrel{(53)}{\leq} \|L^{(U^\uparrow)}(\mathbf{q}_2[0]) - \bar{\mathbf{q}}_1^*\| + \|L^{(U^\downarrow)}(\mathbf{q}_2[N_0 - 1]) - \bar{\mathbf{q}}_1^*\| \\ & \stackrel{(56)}{\leq} \bar{c}^{-1}(2r_{CC} + r_{UE}^{\min}) + \bar{c}^{-1}(r_{CC} + r_{UE}^{\min}) \stackrel{(\text{Lemma 1})}{\leq} \bar{c}^{-1}(r_{CC}). \end{aligned}$$

Therefore, $c(L^{(U^\uparrow)}(\mathbf{q}_2[0]), \hat{\mathbf{q}}_2) \geq r_{CC}$, which establishes C2.

Part 2: Next, UAV-1 follows a shortest path from $L^{(U^\uparrow)}(\mathbf{q}_2[0])$ to $\bar{\mathbf{q}}_1^*$ in \vec{F}_G while UAV-2 stays at $L^{(U^\downarrow)}(\mathbf{q}_2[N_0 - 1])$. Since the flight grid is dense enough, there exists a sequence of adjacent grid points $\vec{p} \triangleq \{L^{(U^\uparrow)}(\mathbf{q}_2[0]), \bar{\mathbf{q}}_1^*[1], \bar{\mathbf{q}}_1^*[2], \dots, \bar{\mathbf{q}}_1^*[\bar{N} - 2], \bar{\mathbf{q}}_1^*\}$ that are sufficiently close to the line segment from $L^{(U^\uparrow)}(\mathbf{q}_2[0])$ to $\bar{\mathbf{q}}_1^*$ so that the rate between the BS and UAV-1 on this path will be at least $c(\mathbf{q}_2[0], \bar{\mathbf{q}}_1^*)$. The combined path is then

$$\begin{aligned} \vec{P}_2 \triangleq & \left\{ \left[L^{(U^\uparrow)}(\mathbf{q}_2[0]), L^{(U^\downarrow)}(\mathbf{q}_2[N_0 - 1]) \right], \right. \\ & \left[\bar{\mathbf{q}}_1^*[1], L^{(U^\downarrow)}(\mathbf{q}_2[N_0 - 1]) \right], \dots, \\ & \left. \left[\bar{\mathbf{q}}_1^*[\bar{N} - 2], L^{(U^\downarrow)}(\mathbf{q}_2[N_0 - 1]) \right], \left[\bar{\mathbf{q}}_1^*, L^{(U^\downarrow)}(\mathbf{q}_2[N_0 - 1]) \right] \right\}. \end{aligned} \quad (59)$$

C1: Since \vec{p} is the set of adjacent grid points approximately on the line segment between $L^{(U^\uparrow)}(\mathbf{q}_2[0])$ and $\bar{\mathbf{q}}_1^*$, it holds that, $\forall \hat{\mathbf{q}}_1 \in \vec{p}$,

$$\|L^{(U^\uparrow)}(\mathbf{q}_2[0]) - \hat{\mathbf{q}}_1\| \leq \|L^{(U^\uparrow)}(\mathbf{q}_2[0]) - \bar{\mathbf{q}}_1^*\|. \quad (60)$$

Squaring both sides and adding $\|\mathbf{q}_{BS} - L^{(U^\uparrow)}(\mathbf{q}_2[0])\|^2$ yields

$$\begin{aligned} & \|\mathbf{q}_{BS} - L^{(U^\uparrow)}(\mathbf{q}_2[0])\|^2 + \|L^{(U^\uparrow)}(\mathbf{q}_2[0]) - \hat{\mathbf{q}}_1\|^2 \\ & \leq \|\mathbf{q}_{BS} - L^{(U^\uparrow)}(\mathbf{q}_2[0])\|^2 + \|L^{(U^\uparrow)}(\mathbf{q}_2[0]) - \bar{\mathbf{q}}_1^*\|^2. \end{aligned} \quad (61)$$

From Pythagoras' theorem, $\forall \hat{\mathbf{q}}_1 \in \vec{p}$, $\|\mathbf{q}_{BS} - \hat{\mathbf{q}}_1\|^2 \leq \|\mathbf{q}_{BS} - \bar{\mathbf{q}}_1^*\|^2$, which in turn implies that

$$c(\mathbf{q}_{BS}, \hat{\mathbf{q}}_1) \geq c(\mathbf{q}_{BS}, \bar{\mathbf{q}}_1^*). \quad (62)$$

Let $\text{proj}(\mathbf{q}) \triangleq [x, y, z_{BS}]^\top$ be the projection of $\mathbf{q} = [x, y, z]^\top$ on the horizontal plane containing the BS. Then, $\text{proj}(\mathbf{q}_1^*) \equiv \text{proj}(\bar{\mathbf{q}}_1^*)$. From Pythagoras' theorem,

$$\|\mathbf{q}_{BS} - \bar{\mathbf{q}}_1^*\|^2 \leq h_{\max}^2 + \|\mathbf{q}_{BS} - \text{proj}(\bar{\mathbf{q}}_1^*)\|^2 \quad (63a)$$

$$= h_{\max}^2 + \|\mathbf{q}_{BS} - \text{proj}(\mathbf{q}_1^*)\|^2 \leq h_{\max}^2 + \|\mathbf{q}_{BS} - \mathbf{q}_1^*\|^2 \quad (63b)$$

$$\stackrel{(52a)}{\leq} h_{\max}^2 + [\bar{c}^{-1}(2r_{CC} + r_{UE}^{\min})]^2 \stackrel{(47)}{\leq} [\bar{c}^{-1}(2r_{CC})]^2. \quad (63c)$$

Hence,

$$c(\mathbf{q}_{BS}, \bar{\mathbf{q}}_1^*) \geq 2r_{CC}. \quad (64)$$

From (62) and (64), $\forall \hat{\mathbf{q}}_1 \in \vec{p}$,

$$c(\mathbf{q}_{BS}, \hat{\mathbf{q}}_1) \geq 2r_{CC}, \quad (65)$$

which proves C1.

C2: Since \vec{p} comprises grid points sufficiently close to the line segment between $L^{(U^\uparrow)}(\mathbf{q}_2[0])$ and $\bar{\mathbf{q}}_1^*$, $\forall \hat{\mathbf{q}}_1 \in \vec{p}$,

$$\|\hat{\mathbf{q}}_1 - \bar{\mathbf{q}}_1^*\| \leq \|L^{(U^\uparrow)}(\mathbf{q}_2[0]) - \bar{\mathbf{q}}_1^*\|. \quad (66)$$

From the triangle inequality, $\forall \hat{\mathbf{q}}_1 \in \vec{p}$,

$$\begin{aligned} & \|\hat{\mathbf{q}}_1 - L^{(U^\downarrow)}(\mathbf{q}_2[N_0 - 1])\| \\ & \leq \|\hat{\mathbf{q}}_1 - \bar{\mathbf{q}}_1^*\| + \|\bar{\mathbf{q}}_1^* - L^{(U^\downarrow)}(\mathbf{q}_2[N_0 - 1])\| \end{aligned} \quad (67a)$$

$$\stackrel{(66)}{\leq} \|L^{(U^\uparrow)}(\mathbf{q}_2[0]) - \bar{\mathbf{q}}_1^*\| + \|\bar{\mathbf{q}}_1^* - L^{(U^\downarrow)}(\mathbf{q}_2[N_0 - 1])\|. \quad (67b)$$

Then, from (67b), (56), and Lemma 1, $\forall \hat{\mathbf{q}}_1 \in \vec{p}$,

$$\begin{aligned} & \|\hat{\mathbf{q}}_1 - L^{(U^\downarrow)}(\mathbf{q}_2[N_0 - 1])\| \\ & \stackrel{(67b)}{\leq} \|L^{(U^\uparrow)}(\mathbf{q}_2[0]) - \bar{\mathbf{q}}_1^*\| + \|\bar{\mathbf{q}}_1^* - L^{(U^\downarrow)}(\mathbf{q}_2[N_0 - 1])\| \\ & \stackrel{(56)}{\leq} \bar{c}^{-1}(2r_{CC} + r_{UE}^{\min}) + \bar{c}^{-1}(r_{CC} + r_{UE}^{\min}) \stackrel{\text{Lemma 1}}{\leq} \bar{c}^{-1}(r_{CC}). \end{aligned}$$

Therefore,

$$c(\hat{\mathbf{q}}_1, L^{(U^\downarrow)}(\mathbf{q}_2[N_0 - 1])) \geq r_{CC}, \quad (69)$$

which proves C2.

Landing subpath (p^\downarrow): The landing path of UAV-2 is $p^\downarrow = \{L^{(U^\downarrow)}(\mathbf{q}_2[N_0 - 1]), L^{(U^\downarrow - 1)}(\mathbf{q}_2[N_0 - 1]), \dots, \mathbf{q}_2[N_0 - 1]\}$. Let $U_1^\downarrow \triangleq \min\{u \in \mathbb{N} : L^{(u)}(\mathbf{q}_1^*) = L^{(u+1)}(\mathbf{q}_1^*) \triangleq \bar{\mathbf{q}}_1^*\}$.

If $U^\downarrow \leq U_1^\downarrow$, \mathbf{q}_1^* has a lower altitude than $\mathbf{q}_2[N_0 - 1]$ and $L^{(U_1^\downarrow - U^\downarrow)}(\mathbf{q}_1^*)$ and $\mathbf{q}_2[N_0 - 1]$ are at the same height. The case when $U^\downarrow > U_1^\downarrow$ can be proven similarly. With $U^\downarrow \leq U_1^\downarrow$, the UAVs descend simultaneously following the combined subpath

$$P_1^\downarrow \triangleq \left\{ \left[L^{(U_1^\downarrow)}(\mathbf{q}_1^*), L^{(U^\downarrow)}(\mathbf{q}_2[N_0 - 1]) \right], \right. \\ \left[L^{(U_1^\downarrow - 1)}(\mathbf{q}_1^*), L^{(U^\downarrow - 1)}(\mathbf{q}_2[N_0 - 1]) \right], \dots, \\ \left[L^{(U_1^\downarrow - U^\downarrow + 1)}(\mathbf{q}_1^*), L^{(1)}(\mathbf{q}_2[N_0 - 1]) \right], \\ \left. \left[L^{(U_1^\downarrow - U^\downarrow)}(\mathbf{q}_1^*), \mathbf{q}_2[N_0 - 1] \right] \right\}. \quad (70)$$

After that UAV-1 continues its descent while UAV-2 stays at $\mathbf{q}_2[N_0 - 1]$. The second combined subpath is then

$$P_2^\downarrow \triangleq \left\{ \left[L^{(U_1^\downarrow - U^\downarrow)}(\mathbf{q}_1^*), \mathbf{q}_2[N_0 - 1] \right], \right. \\ \left[L^{(U_1^\downarrow - U^\downarrow - 1)}(\mathbf{q}_1^*), \mathbf{q}_2[N_0 - 1] \right], \dots, \\ \left. \left[L^{(1)}(\mathbf{q}_1^*), \mathbf{q}_2[N_0 - 1] \right], [\mathbf{q}_1^*, \mathbf{q}_2[N_0 - 1]] \right\}. \quad (71)$$

C1: Proving C1 amounts to showing that $c(\mathbf{q}_{BS}, L^{(u)}(\mathbf{q}_1^*)) \geq 2r_{CC}$ for $u = 0, \dots, U_1^\downarrow$. It is easy to see that

$$c(\mathbf{q}_{BS}, L^{(u)}(\mathbf{q}_1^*)) \geq \min \left[c(\mathbf{q}_{BS}, L^{(0)}(\mathbf{q}_1^*)), c(\mathbf{q}_{BS}, L^{(U_1^\downarrow)}(\mathbf{q}_1^*)) \right] \\ = \min \left[c(\mathbf{q}_{BS}, \mathbf{q}_1^*), c(\mathbf{q}_{BS}, \bar{\mathbf{q}}_1^*) \right]. \quad (72)$$

From (51), it follows that $c(\mathbf{q}_{BS}, \mathbf{q}_1^*) \geq 2r_{CC} + r_{UE}^{\min} > 2r_{CC}$. On the other hand, from (64), it follows that $c(\mathbf{q}_{BS}, \bar{\mathbf{q}}_1^*) \geq 2r_{CC}$. Hence, C1 is proven for P_1^\downarrow and P_2^\downarrow .

C2: One has, $\forall u = 0, \dots, U^\downarrow$, $\|L^{(U_1^\downarrow - u)}(\mathbf{q}_1^*) - L^{(U^\downarrow - u)}(\mathbf{q}_2[N_0 - 1])\| \leq \|\mathbf{q}_1^* - \mathbf{q}_2[N_0 - 1]\|$, then,

$$c(L^{(U_1^\downarrow - u)}(\mathbf{q}_1^*), L^{(U^\downarrow - u)}(\mathbf{q}_2[N_0 - 1])) \geq c(\mathbf{q}_1^*, \mathbf{q}_2[N_0 - 1]) \\ \stackrel{(51)}{\geq} r_{CC} + r_{UE}^{\min} > r_{CC}, \quad (73)$$

which proves C2 for P_1^\downarrow .

In P_2^\downarrow , UAV-1 descends from $L^{(U_1^\downarrow - U^\downarrow)}(\mathbf{q}_1^*)$ to \mathbf{q}_1^* while UAV-2 stays at $\mathbf{q}_2[N_0 - 1]$. Start by noting that $L^{(u)}(\mathbf{q}_1^*)$ is between \mathbf{q}_1^* and $L^{(U_1^\downarrow - U^\downarrow)}(\mathbf{q}_1^*)$, $\forall u = 0, \dots, U_1^\downarrow - U^\downarrow$, which means that

$$\|L^{(u)}(\mathbf{q}_1^*) - L^{(U_1^\downarrow - U^\downarrow)}(\mathbf{q}_1^*)\|^2 \leq \|\mathbf{q}_1^* - L^{(U_1^\downarrow - U^\downarrow)}(\mathbf{q}_1^*)\|^2. \quad (74)$$

From Pythagoras' theorem,

$$\|L^{(u)}(\mathbf{q}_1^*) - \mathbf{q}_2[N_0 - 1]\|^2 = \|L^{(u)}(\mathbf{q}_1^*) - L^{(U_1^\downarrow - U^\downarrow)}(\mathbf{q}_1^*)\|^2 \\ + \|L^{(U_1^\downarrow - U^\downarrow)}(\mathbf{q}_1^*) - \mathbf{q}_2[N_0 - 1]\|^2 \\ \stackrel{(74)}{\leq} \|\mathbf{q}_1^* - L^{(U_1^\downarrow - U^\downarrow)}(\mathbf{q}_1^*)\|^2 + \|L^{(U_1^\downarrow - U^\downarrow)}(\mathbf{q}_1^*) - \mathbf{q}_2[N_0 - 1]\|^2 \\ = \|\mathbf{q}_1^* - \mathbf{q}_2[N_0 - 1]\|^2. \quad (75)$$

It follows that $c(L^{(u)}(\mathbf{q}_1^*), \mathbf{q}_2[N_0 - 1]) \geq c(\mathbf{q}_1^*, \mathbf{q}_2[N_0 - 1]) \geq r_{CC} + r_{UE}^{\min} > r_{CC}$, where the second inequality follows from (51). This proves C2 for P_2^\downarrow .

The case when $U^\downarrow > U_1^\downarrow$, i.e., \mathbf{q}_1^* has a higher altitude than $\mathbf{q}_2[N_0 - 1]$, can be proven similarly.

APPENDIX C PROOF OF LEMMA 1

Let $a \triangleq r_{CC}/B > 0$ and $\ell \triangleq r_{UE}^{\min}/r_{CC}$. Then $(2r_{CC} + r_{UE}^{\min})/B = (2 + \ell)r_{CC}/B = (\ell + 2)a$ and $(r_{CC} + r_{UE}^{\min})/B = (1 + \ell)r_{CC}/B = (\ell + 1)a$. From (7), $\forall r > 0$, it follows that

$$\bar{c}^{-1}(r) \triangleq \left(\frac{A}{2r/B - 1} \right)^{1/\beta}, \quad (76)$$

where $A \triangleq P_t G_t G_r \lambda^\beta / [\sigma^2 (4\pi)^\beta]$. As a result,

$$\bar{c}^{-1}(2r_{CC} + r_{UE}^{\min}) + \bar{c}^{-1}(r_{CC} + r_{UE}^{\min}) \\ = \left(\frac{A}{2^{(\ell+2)a} - 1} \right)^{1/\beta} + \left(\frac{A}{2^{(\ell+1)a} - 1} \right)^{1/\beta}. \quad (77)$$

Since $a > 0$, one has that $(\ell + 2)a > (\ell + 1)a$, which in turn implies that

$$\left(\frac{A}{2^{(\ell+2)a} - 1} \right)^{1/\beta} < \left(\frac{A}{2^{(\ell+1)a} - 1} \right)^{1/\beta}. \quad (78a)$$

It follows that

$$\bar{c}^{-1}(2r_{CC} + r_{UE}^{\min}) + \bar{c}^{-1}(r_{CC} + r_{UE}^{\min}) \\ < 2 \left(\frac{A}{2^{(\ell+1)a} - 1} \right)^{1/\beta}. \quad (79)$$

By hypothesis,

$$r_{UE}^{\min} \geq B \log_2 (1 + 2^\beta \text{SNR}_{CC}^{\min}) \quad (80a)$$

$$- B \log_2 (1 + \text{SNR}_{CC}^{\min}) \\ = B \log_2 \left(2^\beta (2^{r_{CC}/B} - 1) + 1 \right) - r_{CC} \quad (80b)$$

$$(80c)$$

Then,

$$\ell = \frac{r_{UE}^{\min}}{r_{CC}} \geq \frac{B}{r_{CC}} \log_2 \left(2^\beta (2^{r_{CC}/B} - 1) + 1 \right) - 1 \quad (81a)$$

$$= \frac{1}{a} \log_2 \left(2^\beta (2^a - 1) + 1 \right) - 1. \quad (81b)$$

Simple algebraic manipulations yield

$$\frac{2^\beta}{2^{a(\ell+1)} - 1} \leq \frac{1}{2^a - 1}, \quad (82)$$

which implies that

$$2 \left(\frac{A}{2^{(\ell+1)a} - 1} \right)^{1/\beta} \leq \left(\frac{A}{2^a - 1} \right)^{1/\beta} = \bar{c}^{-1}(r_{CC}). \quad (83)$$

Combining (79) and (83) yields (57).

APPENDIX D
PROOF OF THEOREM 2

This proof follows a similar logic to the one in the proof of Theorem 1. Algorithm 5 fails iff there is no path for UAV-1 that results in a feasible combined path at all iterations, in particular at the U -th iteration, where $U \triangleq \min\{u : \bar{L}^{(u)}(p_2) = \bar{L}^{(u+1)}(p_2)\}$. Therefore, it suffices to show that there exists a path for UAV-1 (not necessarily the one produced by Algorithm 5) that results in a feasible combined path when UAV-2 follows $\bar{L}^{(U)}(p_2)$. To this end, a path will be designed for UAV-1 and the combined path $P \triangleq \{\dot{\mathbf{Q}}[0], \dots, \dot{\mathbf{Q}}[N_{\text{UE}} - 1]\}$, where $\dot{\mathbf{Q}}[n] \triangleq [\dot{\mathbf{q}}_1[n], \dot{\mathbf{q}}_2[n]]$ and $\{\dot{\mathbf{q}}_2[0], \dots, \dot{\mathbf{q}}_2[N_{\text{UE}} - 1]\} = \bar{L}^{(U)}(p_2)$ will be shown to be feasible. This means that the following conditions hold:

- C1: The rate between the BS and UAV-1 is at least $2r_{\text{CC}}$, i.e., $c(\mathbf{q}_{\text{BS}}, \dot{\mathbf{q}}_1[n]) \geq 2r_{\text{CC}}$ for all n , and
 C2: The rate from UAV-1 to UAV-2 is at least r_{CC} , i.e., $c(\dot{\mathbf{q}}_1[n], \dot{\mathbf{q}}_2[n]) \geq r_{\text{CC}}$ for all n .

To simplify the exposition, the path $\bar{L}^{(U)}(p_2)$ will be separated into the following subpaths:

$$\begin{aligned} p^\uparrow &\triangleq \{\mathbf{q}_2[0], L^{(1)}(\mathbf{q}_2[0]), \dots, L^{(u_{\text{max}}^\uparrow)}(\mathbf{q}_2[0])\}, \\ \vec{p} &\triangleq \{L^{(u_{\text{max}}^\uparrow)}(\mathbf{q}_2[0]), \bar{\mathbf{q}}_2[1], \dots, \bar{\mathbf{q}}_2[N_{\text{UE}} - u_{\text{max}}^\uparrow - 1]\}, \end{aligned} \quad (84)$$

where $p_2 \triangleq \{\mathbf{q}_2[0], \mathbf{q}_2[1], \dots, \mathbf{q}_2[N_{\text{UE}} - 1]\}$. For each subpath, a path will be designed for UAV-1 and the resulting combined path will be shown to satisfy C1 and C2. The designed path is illustrated in Fig. 15.

Take-off subpaths (p^\uparrow): In the considered combined path, when UAV-2 follows p^\uparrow , UAV-1 follows p^\uparrow as well. Recall that the minimum separation between the UAVs was disregarded in (8) for simplicity. Thus, the combined path of UAV-1 and UAV-2 is given by

$$\begin{aligned} P^\uparrow &\triangleq \left\{ [\mathbf{q}_2[0], \mathbf{q}_2[0]], [L^{(1)}(\mathbf{q}_2[0]), L^{(1)}(\mathbf{q}_2[0])], \dots, \right. \\ &\quad \left. [L^{(u_{\text{max}}^\uparrow)}(\mathbf{q}_2[0]), L^{(u_{\text{max}}^\uparrow)}(\mathbf{q}_2[0])] \right\}. \end{aligned} \quad (85)$$

C1: By hypothesis, $h_{\text{max}} \leq \bar{c}^{-1}(2r_{\text{CC}})$. Thus, since $\mathbf{q}_2[0] = \mathbf{q}_{\text{BS}}$, $\forall \dot{\mathbf{q}}_1 \in p^\uparrow$, it follows that $\|\mathbf{q}_{\text{BS}} - \dot{\mathbf{q}}_1\| \leq \|\mathbf{q}_{\text{BS}} - L^{(u_{\text{max}}^\uparrow)}(\mathbf{q}_2[0])\| \leq h_{\text{max}} \leq \bar{c}^{-1}(2r_{\text{CC}})$. Noting that c is a decreasing function of the distance yields

$$c(\mathbf{q}_{\text{BS}}, \dot{\mathbf{q}}_1) \geq c\left(\mathbf{q}_{\text{BS}}, L^{(u_{\text{max}}^\uparrow)}(\mathbf{q}_2[0])\right) \geq 2r_{\text{CC}}, \quad (86a)$$

which establishes C1.

C2: trivial.

Top subpath (\vec{p}): In the considered combined path, when UAV-2 follows \vec{p} , UAV-1 stays at $L^{(u_{\text{max}}^\uparrow)}(\mathbf{q}_2[0])$. This results in the following combined path

$$\begin{aligned} P^\uparrow &\triangleq \left\{ [L^{(u_{\text{max}}^\uparrow)}(\mathbf{q}_2[0]), L^{(u_{\text{max}}^\uparrow)}(\mathbf{q}_2[0])], [L^{(u_{\text{max}}^\uparrow)}(\mathbf{q}_2[0]), \bar{\mathbf{q}}_2[1]], \right. \\ &\quad \left. \dots, [L^{(u_{\text{max}}^\uparrow)}(\mathbf{q}_2[0]), \bar{\mathbf{q}}_2[N_{\text{UE}} - u_{\text{max}}^\uparrow - 1]] \right\}. \end{aligned} \quad (87)$$

C1: shown previously.

C2: By definition of U , $[0, 0, 1]\dot{\mathbf{q}}_2 = h_{\text{max}}, \forall \dot{\mathbf{q}}_2 \in \vec{p}$. Also, $\mathbf{q}_2[0] = \mathbf{q}_{\text{BS}}$. This means that $\forall \dot{\mathbf{q}}_2 \in \vec{p}$, $\|L^{(u_{\text{max}}^\uparrow)}(\mathbf{q}_2[0]) - \dot{\mathbf{q}}_2\| \leq dc_{\text{min}} \leq \bar{c}^{-1}(r_{\text{CC}})$. Then $c(L^{(u_{\text{max}}^\uparrow)}(\mathbf{q}_2[0]), \dot{\mathbf{q}}_2) \geq r_{\text{CC}}, \forall \dot{\mathbf{q}}_2 \in \vec{p}$.

APPENDIX E
BENCHMARK 6

In this benchmark, for every N_{replan} time steps, the planner is given the next N_{known} locations of the user, $N_{\text{replan}} \leq N_{\text{known}}$. The following steps will be iteratively implemented at time steps $nN_{\text{replan}}, n = 0, 1, \dots$

- S1: The planner uses the algorithms in Sec. V-A to plan a path for the UAVs to the nearest grid points where they can serve
- All of the next N_{known} locations of the user.
 - If such grid points do not exist, the planner plans a path to the nearest grid points where the UAVs can serve the last $(N_{\text{known}} - 1)$ known locations of the user, i.e., $\mathbf{q}_{\text{UE}}[nN_{\text{replan}} + i], i = 1, \dots, N_{\text{known}} - 1$, and so on.
 - In the most extreme case when the planner cannot find grid points to simultaneously guarantee $r_{\text{UE}}^{\text{min}}$ to multiple locations of the user, the planner plans a path to the nearest grid point where the UAVs can serve the last known location of the user, i.e., $\mathbf{q}_{\text{UE}}[nN_{\text{replan}} + N_{\text{known}} - 1]$.
- S2: If the length of the path obtained in Step 1 is less than N_{replan} , the last configuration point of the path is repeated until the length of the path is N_{replan} . If the length of the path obtained in Step 1 is greater than N_{replan} , only the first N_{replan} configuration points of the path are kept.
- S3: The last configuration point of the path obtained in Step 2 provides the start locations of the UAVs in the next iteration, i.e., at time step $(n + 1)N_{\text{replan}}$.